U.S. Department of Commerce
National Oceanic and Atmospheric Administration
National Weather Service
National Centers for Environmental Prediction
5200 Auth Road
Camp Springs, MD 20746-4304

Office Note 467

A standardized procedure for the derivation of smooth and partially overset grids on the sphere, associated with polyhedra that admit regular griddings of their surfaces. Part I: Mathematical principles of classification and construction

R. James Purser* and Miodrag Rančić
IM Systems Group, Rockville, Maryland

December 15, 2011

* email: jim.purser@noaa.gov

1. Introduction

Modern global grid point models of the atmosphere are not well served by the traditional horizontal grids based on the latitude and longitude coordinate framework. The character and stability of the numerical solutions on such a grid are radically and adversely affected by the excessive east-west resolution of the grid at high latitudes, unless the models invoke a strong low-pass spatial filter at every time step. These unwelcome features of the latitude-longitude grid have been acknowledged and understood for many years and, although various remedial measures have been devised to ameliorate the time step restrictions and other problems caused by the convergence of meridians at the poles, the results are often less than satisfactory. With the widespread adoption of massively parallel computation, and the consequent need to apportion different parts of the horizontal grid to separate communicating processors, new difficulties associated with the latitude-longitude grids emerge. Near the poles, relatively short geographical distances can be very many grid units apart, making the practical problem of subdividing the grid for efficient parallel processing an extremely challenging one. Using a latitude-longitude grid in which the stored values are progressively thinned in the zonal direction as one moves to successively higher latitudes (e.g., Gates and Riegel 1962; Kurihara 1965) is a strategy that successfully addresses the problem of achieving a more homogeneous horizontal distribution, but at the considerable cost of incurring severe difficulties in performing any numerical operations normally carried out along meridians.

Many alternative grid geometries have been proposed and investigated for global meteorological applications. A review of many of these alternative geometries and a discussion of their merits and their drawbacks will be found in Staniforth and Thuburn (2012). The locally triangular grid of data (locally hexagonal grid cells) that employs a global subdivision based on the regular icosahedron (twenty equilateral triangular faces with twelve vertices) seems first to have been proposed for meteorological applications by Sadourny et al. (1968), Williamson (1968, 1970), and extended to a finite element formulation by Cullen (1974). This class of grids was revived, with evident success, by Baumgardner and Frederickson (1985) who used this structure for investigations of mantle convection, and, for meteorological applications, by Masuda and Ohnishi (1986), Heikes and Randall (1995a, 1995b), Thuburn (1997), Giraldo (1997), Majewski (1998) and Lee et al. (2007). We shall refer to the local geometry of such grids as 'triangular', referring to the shape of the basic circuits exhibited by the network of links between adjacent grid cells (most of which, having six neighbors, are conventionally depicted as hexagonal). Also, we implicitly assume henceforth that by 'triangular grid' we refer to *equilateral* triangles in the decomposition. The triangular grids have the theoretical advantage of possessing a more isotropic resolution than a locally quadrilateral grid, although the indexing of data points and the implementation of numerical differencing schemes tends to become a little more involved. The icosahedron is the regular polyhedron or 'Platonic solid' (e.g., Coxeter 1973) sharing with the non-griddable regular dodecahedron the highest possible degree of symmetry. This leads to a naturally high degree of grid homogeneity and relative lack of distortion, even with rather simple grid construction techniques.

Among locally quadrilateral grids, the simplest and most symmetrical global geometry that avoids the problems of the latitude-longitude arrangement is the 'cubed sphere' class derived from some projection of the surface of the cube onto the sphere. An approach of this kind

was pioneered by Sadourny (1972) and, in the new era of massively parallel computation, has once again emerged in the work of Ronchi et al. (1996), Rančić et al. (1996) and McGregor (1996), where the relative ease of partitioning this grid among many processors is fully exploited. Thomas and Loft (2000) employ the cubic arrangement for their global implementation of a spectral element model, combining some of the best features of spectral and grid-based methods. Putman and Lin (2007) employ the cubic sphere framework for their finite volume method, although the intrinsic regularity of the cubic grid is not directly exploited in the finite volume context.

Other, less symmetrical geometries also admit a locally quadrilateral gridding. Purser and Rančić (1997) proposed an octahedral dihedron (that is, a flat two-faced polyhedron) which, like the cubic arrangement, results in eight 'corner singularities'. This octagonal geometry removes singularities from the middle latitudes controlled by the baroclinic instabilities, where simulation may to some extent be adversely affected by the nature of the singularities, and puts them all in a quasi-regular pattern around the equator where atmospheric dynamics is mostly dictated by convection. Note that there is a corresponding dodecagonal (12-sided) dihedron configuration for the triangular grid.

These various polyhedral mappings of the sphere assume that the global grid consists of several subgrids that perfectly match each other at the boundaries. One consequence of such a choice is that the global grid has singular points. Another is that, following any effort made to equalize the effective grid element areas in these configurations over the entire domain, the grid necessarily becomes nonorthogonal. In that case, a general curvilinear formulation of the governing equations becomes unavoidable. Among other issues arising from a nonorthogonal grid are obstacles impeding the direct adaptation of existing orthogonal-grid numerical models (e.g., Zhang and Rančić, 2007), and the adoption of a 'strong conservative form', which is generally prefered in contemporary numerical models (e.g., Rančić et al., 2008). A general (nonorthogonal) curvilinear formulation includes 'cross terms' of the metric, whose presence generally degrades the accuracy of numerical schemes. On a positive note, mappings with smoothly matched subgrid elements enables one, relatively easily, to achieve global conservation of various important integral properties. However, if one decides to relax the requirement for perfect matching of elementary subgrids, then the spectrum of options for mapping of the sphere vastly increases, but with the price paid being the loss of formal conservation (or at least, an easy way to achieve it). The technique of overlapped ('Chimera', or 'overset') grids, pioneered in Starius (1980), Chesshire and Henshaw (1990), and Henshaw (1994), is successfully used for integration over complex domains in a variety of problems in computational fluid dynamics. In atmospheric science, attempts to cover the whole globe with overlapping grids may be found in Phillips (1957), Browning et al. (1989), Ronchi et al. (1996) and Rančić and Zhang (2006). As we shall see, the application of the oversetting technique near the polyhedral corner singularities mitigates the most salient disparities of grid element areas, and, for the square grid types at least, can be carried out in a way that allows the resulting computational grid to retain the desirable property of exact orthogonality with all the numerical advantages this implies.

In Section 2 of this note we attempt first to answer the following question:

(i) Which polyhedra lead to potentially useful global grids?

In Section 3 we discuss the topic of 'symmetry groups' and answer the questions:

(ii) What symmetries do the different polyhedral grid systems have in common?

(iii) What are the characteristic merits of each polyhedral grid?

Map distortion tends to be minimized by positioning the vertices mutually as far apart as possible. Polyhedra with high orders of symmetry tend to succeed in this respect. All the most symmetrical polyhedra have a unique form; they are the regular solids known from antiquity. But some of our less symmetrical polyhedral types encompass a continuous range of shapes generally distinguished by an aspect ratio of two (or, in some instances, three) integer parameters (possibly with other consistency inequality constraints). An example, is when it is the ratio of the alternating sides (in appropriate map panel units) that defines the degree of zonal anisotropy of an octagonal or a dodecagonal dihedron. In such cases we would ask the additional question, which Section 4 seeks to answer using the theory of 'Pell' equations:

(iv) What are the most judicious choices of aspect ratios that imply the most advantageous (symmetrical?) polyhedra of each type, given a cap on the number of congruent map panels we are willing to allow?

Once the choice of polyhedral shape has been determined for a given application we are confronted with the problem of how to map the surface of the polyhedron to the sphere. Conforming to all the symmetries possessed by the original polyhedron certainly imposes many helpful constraints but still leaves a great deal of ambiguity unless we adopt additional guiding principles. The mathematically most elegant solution is to conformally map the polyhedral surface to the sphere since the symmetry-preserving solution is unique for all the polyhedra considered and the result is a mapping that is, in a certain sense, as smooth as it is possible for the mapping to be. It is especially attractive that the mapping is perfectly smooth across the interiors of all the polyhedron's edges. But the mapping of the grid is still problematic from the stand point of numerical analysis because in the vicinty of every vertex the mapping suffers from both unbounded curvature and a singularity in the map's absolute Jacobian or map factor. In Section 5 we describe a presentation of the conformal mapping equations as the solution of a variational principle written using a three-dimensional Cartesian representation of the points of the sphere that facilitates the numerical solution of this problem in a way that manifestly respects the polyhedral symmetries. We then address the question:

(v) Having chosen a griddable polyhedron is there a *systematic* way to construct a corresponding continuous mapping from its surface to the sphere that respects the original symmetries and provides control over the degree of areal inhomogeneity of the grids implied by this mapping?

What we propose does indeed provide such a systematic procedure and allows precise control over the extent to which conformality is sacrificed in order to improve areal homogeneity. The unavoidable singularities of the continuous mappings are a bane of numerical analysis on the surface of the sphere. They adversely affect spatially differentiation, interpolation, filtering, and, in more subtle ways, even the horizontal integration of the gridded variables. For many such applications it is vitally important that there be *no* singularity present anywhere within the portion of the grid where the numerical operators need to be applied. The proposed remedy is to incorporate incisions that transect each vertex, but without violating the integrity of any of the map panels that meet there. Adjustment of the geometry on either side of the incision allows us to completely remove the original angular discontinuity. In Section 6 we treat the question:

(vi) Given the polyhedral mapping with areal disparities adequately rectified according

to the principles set out in Section 5, is there a *systematic* prescription for constructing the necessary oversets that eliminates the remaining curvature discontinuities associated with the vertices of the original polyhedron?

In our affirmative response we again formulate generic procedures, expressed in the three-dimensional Cartesian domain in a way that guarantees that the intended symmetries are numerically respected.

The concluding discussion of Section 7 reviews the implications of the standardization of symmetry-preserving polyhedral grids that is the main focus of this note. But we also argue that the slavish adherence to the rigorous dictates of symmetry at *all* levels of the grid creation process can sometimes detrimentally limit the opportunities available for constructing global grids with advantageous features. We illustrate this point by showing how one can exploit the theory of Pell equations discussed in Section 4, together with a generalization of the overset technique (Starius 1980, Browning et al. 1989) for map regions overlapping *three* at a time, to enable an orthogonal and almost-square rectangular gridding to be applied to a smoothly mapped *spherical icosahedron*! This counter-intuitive configuration certainly violates the strict symmetry principles as we shift our focus from the global geometry to the local grid geometry, and yet it enables the minimal-distortion attributes of the icosahedral geometry to be nicely combined with the convenience and high numerical efficiency enjoyed by conventional rectangular-grid atmospheric models, providing a configuration that may prove superior in practice to any of the more orthodox and symmetry-respecting polyhedral grids whose classification and construction we have sought to systematize.

The polyhedral grid geometries that we highlight in this note are just a small subset of the possible types for which the vertices are all equivalent to each other under the operations of symmetry that characterize the particular gridding. The appendix classifies all the types of such finite 'vertex-symmetric' polyhedral griddings of both square and triangular types, and provides an illustration of the polygonal 'development', or 'net', of the simplest exemplar of each type.

2. Practical griddable polyhedra

We have discussed how the potentially useful quadrilateral and triangular grids on the sphere which tend to minimize the proportion where the map distortion is large are found to be associated with convex polyhedra. These polyhedra possess relatively high degrees of symmetry, inherited by the spherical mapping, and are such that, on the flat surface of each 'face', the mapping of the grid is uniform and forms either a perfect square lattice, or a perfect equilateral triangular lattice. The vertices of each polyhedron carry equal amounts of angular deficit – the discrete measure of the surface's Gaussian curvature. The global tally of this measure over the surface of any simply-connected polyhedron is necessarily 4π radians, or 720°. Thus, for the icosahedral grid and other global triangular grids with singularities of a similar magnitude of distortion, there are always found to be 12 vertices in the associated convex polyhedron and an angular deficit of 60° at each one. For the cubic grid, and for any other global quadrilateral grids with singularities of a similar degree of distortion to the cube's, the vertex count is always eight and the angular deficit per vertex is 90°.

The grid geometries we have discussed do not exhaust the serviceable possibilities; Fig. 1 exhibits twelve symmetric polyhedral types, the first four of which admit a square surface gridding, while the other eight admit an equilateral triangular surface gridding. Each cartoon of this figure shows one 'half-shell' of the griddable polyhedral surface, displayed cut and flattened ('developed') onto the Euclidean plane, and each subdivided into the respective largest square or triangular 'panels' conditional on vertices of the polyhedron occurring only at vertices (not edge-interiors) of panels. The boundary of the half shell is a great circle that we might think of as one double-meridian; the opposite, missing half-shell being, in every case, the exact mirror-image of the half-shell shown.

To each polyhedron, centered on the Cartesian coordinate origin, is associated a characteristic 'point group' of the three-dimensional orthogonal matrix operators – rotations and reflections – that map the polyhedron, and therefore its associated spherical gridding, into itself. A common property of all the point groups associated with these griddable polyhedra is (at least) two planes of reflection symmetry that are themselves mutually orthogonal. One of these we take as the bisecting plane that cleaves the half-shells of Fig. 1 from their omitted respective opposites; the other reveals itself in the cartoons as the bilateral symmetry axis extending from the top ('North Pole') to the bottom ('South Pole') of each. Thus, the axis of intersection of the two reflection planes are taken here to define the polar axis in the conventional presentation. When a third orthogonal reflection plane also exists, the ambiguity is broken (if possible) by the choice that confers on this polar axis the highest degree of rotational symmetry among the three choices.

Figure panels (a)—(d) show the half-shell types for most of the polyhedra admitting square griddings that enjoy some potential merits when realized as spherical griddings for numerical weather prediction. Fig. 1(a) shows the development of the basic cube, whose shape is unique and needs no further specification. The short thick segments transecting each vertex in this and the other cartoons indicates the loci of the 'cuts' in suggested overset versions of the polyhedral map. For this cubic case, the oversets shown are those that would yield a grid of the 'Yin-Yang' variety (Kageyama and Sato 2004, Purser 2004) but an alternative arrangement of oversets gives the equally attractive 'barrel grid' configuration. A less symmetrical generalization of the cube, maintaining the mutually orthogonal 'Cartesian' symmetry planes, would be the square prism, and an even less symmetrical generalization of that would be the general cuboid. Another way in a which a given griddable geometry can be generalized is by the choice of orientation of the grid with respect to the mirror-symmetry planes of the polyhedron. For the cube, square prism and cuboid, a distinction can be made between the gridding whose lines are parallel to the edges and the griddings aligned at 45° to these edges, even though the same group of polyhedral symmetries is in effect. But other oblique alignments of the surface gridding of these polyhedra are also possible; however, these oblique griddings are no longer invariant to the improper rotational symmetries of the polyhedron. Moreover, in the case of a general cuboid, not only is the size of the symmetry group thereby halved, but the eight vertices of this chiral configuration are now no longer equivalent under the smaller group of symmetries available (disqualifying this configuration from the classification given in the appendix, which is restricted to a full classifications of only *vertex-symmetric* polyhedral grid types). We shall only explicitly consider the simplest of the possible grid orientations in each of the geometries featured in Fig. 1 but it is important to bear in mind the existence of the alternative orientations

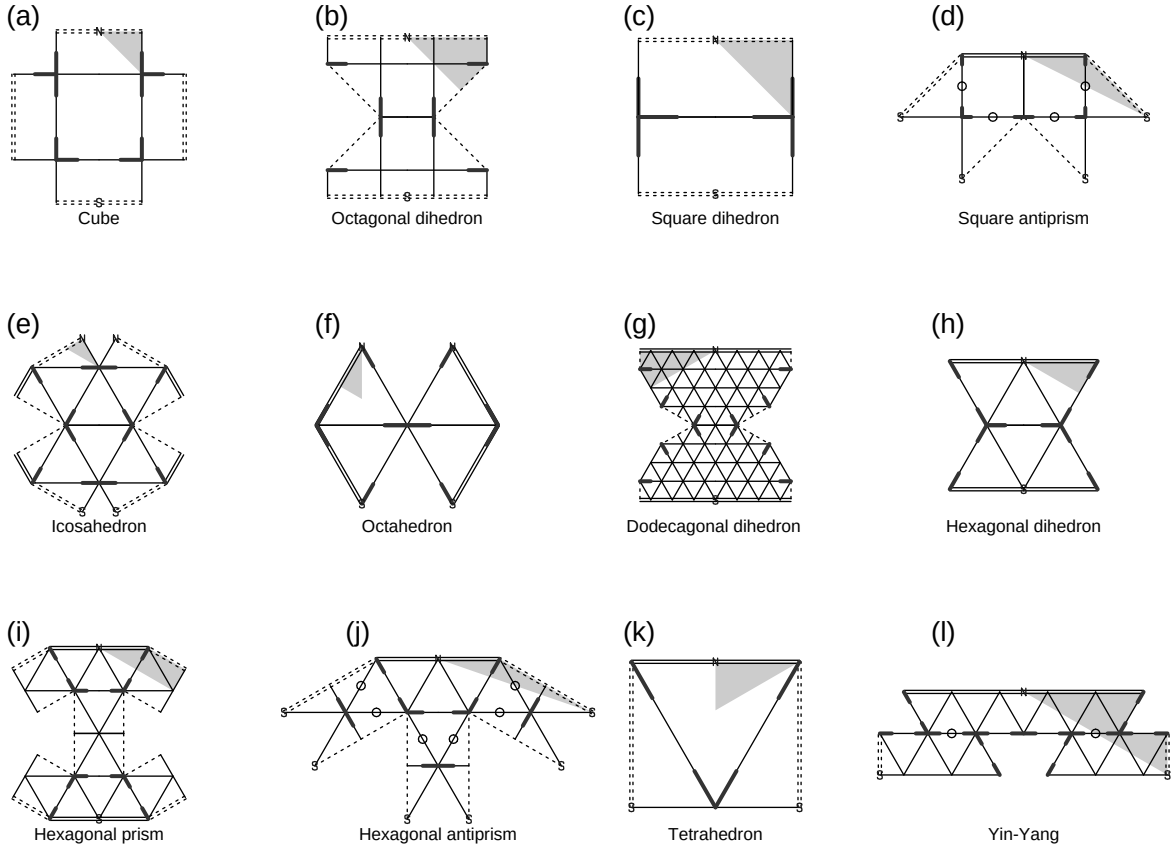

Figure 1. Half-shells of twelve mirror-symmetric polyhedra that allow regular griddings of their surfaces by either square (a—d) or triangular (e—l) grids. Each half-shell is suitably cut to allow it to be developed (without further distortion) to the plane, and presented so as to exhibit its other mirror-reflection symmetry bilaterally, with the intersection of the two chosen symmetry planes forming the polar axis. The poles themselves in this standard presentation are indicated in each figure by small symbols 'N' and 'S'. Thin solid lines are the boundaries of square or equilateral map-panels, dotted lines are cuts not conforming to these panel boundaries. Short bold segments mark 'cuts' between sets of map panels that allow the otherwise singular vertices of the mapping of these panels to the sphere to be replaced, via a local stretching of the maps involved, by corner-oversets that allow the mathematical singularities at these corners to be removed. The lines are doubled to indicate where they reside within the plane of mirror symmetry. The locations of any axes of period-two gyration *not* also within mirror symmetry planes are indicated by the small circles. In each developed half-shell a representative 'fundamental region' of the symmetry is shaded in grey.
The polyhedra are as follows: (a) cube (cuts shown for Yin-Yang-style oversets); (b) octagonal dihedron; (c) square dihedron; (d) square antiprism; (e) icosahedron; (f) regular octahedron; (g) dodecagonal dihedron; (h) hexagonal dihedron; (i) hexagonal prism; (j) hexagonal antiprism; (k) regular tetrahedron; (l) Yin-Yang (irregular) octahedron. The full list of vertex-symmetric polyhedral grid types is provided in the appendix.

which might sometimes, for practical reasons, be preferred.

Cartoon (b) shows one of the family of octagonal dihedra where now the exact shape requires further specification, since the octagon sides parallel and orthogonal to the sides of adjacent square map panels can be one integer in length, while the alternating sides at 45° can be $\sqrt{2}$ times some other integer. Cartoon (c) shows the square dihedron; although it shares the same symmetries as the octagonal dihedron and, in some respects can be thought of as a degenerate member of that family, it must be noted that it has only *four* vertices, so each must carry

the double dose of a 180° angular deficit. This implies that its map singularities must be, in some sense, twice as strong as those for the other square-griddable polyhedra, so we shall expect a much more severe degree of map distortion around each of its map singularities. Cartoon (d) shows one of an infinite family of square 'antiprisms'; this simplest example is formed from the gluing together of two large squares (each possessing four map panels since the large squares themselves are disqualified from being 'panels' by having polyhedron vertices at the midpoints of their sides). But other square antiprisms exist with different aspect ratios (degrees of oblateness/prolateness) so an exact specification of shape (like the octagons) requires a pair of integer aspect parameters.

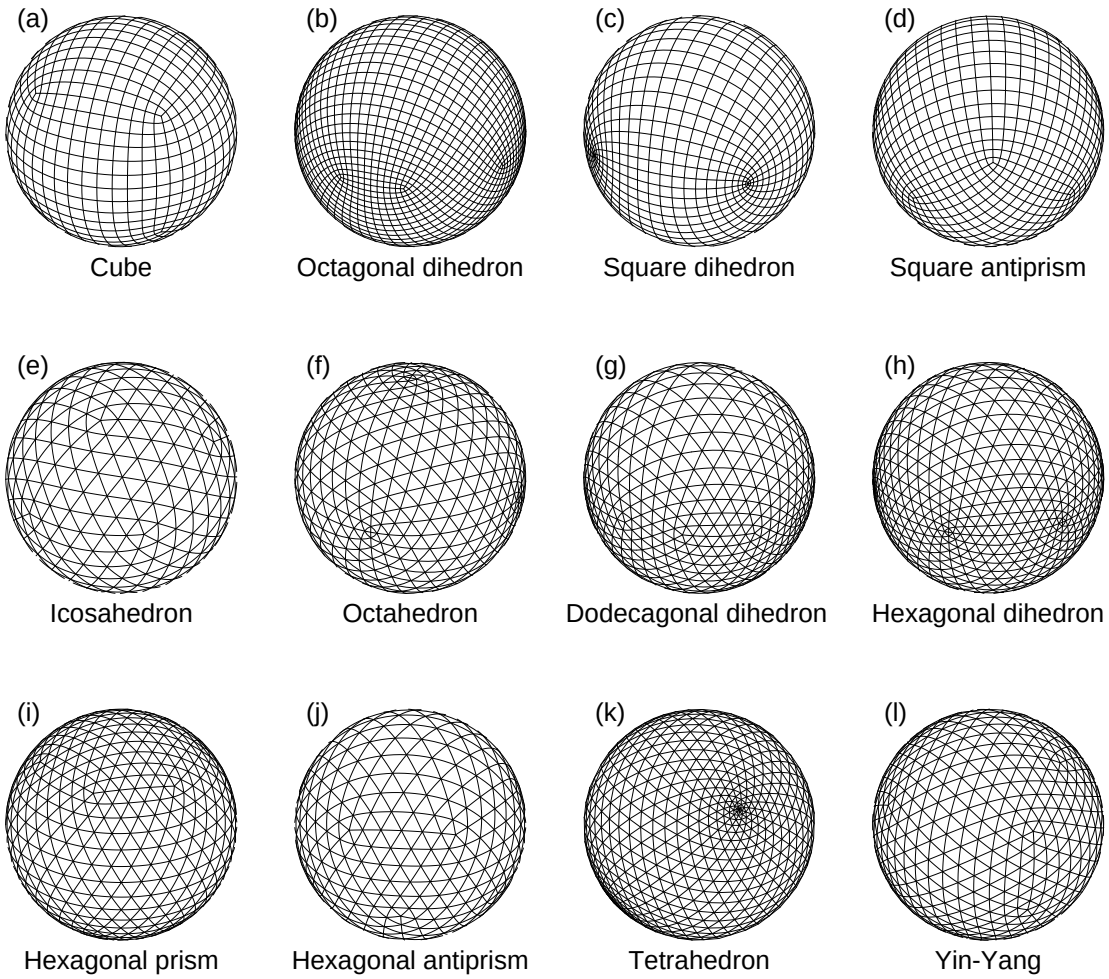

Figure 2. Conformal mapping grids on the sphere corresponding to the polyhedra shown in Fig. 1. The grids are depicted as viewed from an oblique angle. Obviously, the schematic grids shown are extremely coarse, but they do give an idea of the qualitative nature of the singularities and their relative positions on the surface.

The panels (e)—(ℓ) of Fig. 1 all depict the half-shells of the polyhedra that admit equilateral triangular surface gridding. Cartoon (e) shows the regular icosahedron (20 panels), the most symmetrical configuration of them all, while (f) shows another Platonic form – the regular octahedron, whose six vertices are each of double strength (angular deficit of 120° as opposed

to the icosahedron's 60° vertex angular deficits). Cartoon (g) shows one of the many possible dodecagonal dihedra. The shape shown clearly exhibits a remarkably high degree of zonal isotropy, but at the cost of requiring 180 congruent map panels. In (h) we see the degenerate version of the dodecagon in the form of the hexagonal dihedron with its six double-strength singularities, each with a 120° angular deficit. Panels (i) and (j) show the simplest representatives of the infinite families of hexagonal prisms and antiprisms, needing respectively 36 and 24 map panels in the particular cases shown. With just four map panels and four triple-strength vertex singularities, (k) shows the regular tetrahedron. The best overset version of this grid yields another 'Yin-Yang' configuration. Completing this survey, (ℓ) shows the half-shell of a 'Yin-Yang' triangular-griddable polyhedron (actually a highly irregular octahedron comprising four rectangles and four irregular pentagons for faces). This configuration needs 36 map panels. However, the vertices of this polyhedron are of two inequivalent types (disqualifying this geometry from the catalogue given in the appendix).

The conformal mappings of the coarsely gridded surfaces of the geometries shown in Fig. 1 to the sphere are shown, from an oblique vantage, in Fig. 2.

We have not illustrated square prisms (other than the special case of the cube and the degenerate case of the square dihedron), the triangular prism, or the triangular antiprism (except the special case of the octahedron). Although the generic members of these neglected families seem to possess no special merit for modeling not already possessed in greater measure by members of the other polyhedra shown in Figs. 1 and 2, we can nevertheless find all of the vertex-symmetric grid geometries listed in the appendix and we emphasize that each one of them can be mapped to the sphere in accordance with the principles we set out in the sections that follow. We will discuss some of the merits of selected grids at the end of the next section, after we have explored the topic of symmetry and the formalism, Group Theory, employed to systematize it.

3. Symmetry Groups associated with polyhedra

The griddable polyhedra that are potentially useful for supplying global grid geometries are each associated with a (maximal) group whose 'elements' are orthogonal transformations with respect to which the polyhedron is invariant. An orthogonal transformation in three dimensions is either a 'positive-parity' chirality-preserving proper rotation about some axis, or the product of such a rotation with a chirality-reversing inversion through the origin (a 'negative-parity' improper rotation). The matrix representation of the former has determinant $+1$ and that of the latter has determinant -1.

In order to specify a group unambiguously, it suffices to specify a subset (just two or three for these polyhedral groups) of the group elements, known as 'generators', from which the full group is recovered by closure under multiplicative combination (remembering, of course, that group operations are not, in general, commutative). By itself, any polyhedral group element serves as the generator of a finite cyclic group so, without any loss in generality, we can choose the representative generator of any cyclic group to be one of its elements whose positive-parity part corresponds to the smallest nonvanishing rotation angle for that cyclic group. If that characterizing angle is $2\pi/N$, for positive integer N and the axis is in the direction (g_x, g_y, g_z)

then we shall specify that generator, G (and hence its corresponding cyclic group), by the notation:

$$G \equiv \begin{cases} [g_x, g_y, g_z]_{+N} & : \text{ if a proper rotation} \\ [g_x, g_y, g_z]_{-N} & : \text{ if an improper rotation} \end{cases} \tag{3.1}$$

If the suffix is of the form '$-N$' for *odd* N, then the order of the cyclic group thus indicated is $2N$; in all other cases it is N.

TABLE 1. Polyhedra admitting square griddings, their Symmetry Groups, and significant merits. Normally, grids possess eight vertices of angular deficit 90°; $*$ denotes the exceptional grid whose four vertices have angular deficit of 180°.

Polyhedral global grid instances	**Group type**	**Order of group**	**Panel count**	**Significant merits**
Cube	O_h ($\star 432$)	48	6	Highest order of symmetry possible for square gridding
Cubic barrel overset grid	D_{4h} ($\star 224$)	16	6	Preserves cube's D_4 zonal symmetry
Cubic Yin-Yang overset grid	D_{2d} ($2\star 2$)	8	6	Sphere maps to a pair of congruent overlapping rectangles
Pellian sequence of square*/octagonal dihedra.	D_{4h} ($\star 224$)	16	2, 14, 82, $\ldots, Q_{2n+1}, \ldots$	All singularies or oversets confined to equator; approximately order-32 symmetry of D_{8h} for large n.
Square antiprism	D_{4d} ($2\star 4$)	16	8	Sphere maps to a pair of congruent squares

An operation generating a group of order 2 is called an 'involution'; involutory generators are therefore those with suffix: -1 (an inversion through the origin for which the 'axis' is redundant); $+2$ (proper rotation of 180°); or -2 (reflection in the plane through the origin perpendicular to the given axis). It is convenient to name the frequently used reflections associated with the three Cartesian axes:

$$X \equiv [1, 0, 0]_{-2}, \tag{3.2a}$$

$$Y \equiv [0, 1, 0]_{-2}, \tag{3.2b}$$

$$Z \equiv [0, 0, 1]_{-2}. \tag{3.2c}$$

In relating the generators to Fig. 1, we adopt the convention that axis $(1, 0, 0)^\mathsf{T}$ points out of the page, $(0, 1, 0)^\mathsf{T}$ points to the right, and $(0, 0, 1)^\mathsf{T}$ is directed upwards, i.e., towards to North Pole. Although the specified generator never depends on the magnitude of the axis vector (only its direction) we shall nevertheless adopt the convention that the largest component of the axis is $+1$.

There are infinitely many ways of presenting a given group of polyhedral symmetries. However, as already noted, we find that in all the cases of interest to us, there exist at least two (and sometimes three) mutually-orthogonal reflection planes. Consequently we adopt the systematic convention that the presentation of the group is such that reflections, X and Y, both belong

TABLE 2. Polyhedra admitting triangular griddings, their Symmetry Groups, and significant merits. Normally, triangular grids possess 12 vertices of angular deficit 60°; * denotes the exceptional grids whose six vertices have angular deficits of 120°, while ** denotes the grid whose four vertices have an angular deficit of 180°.

Polyhedral global grid instances	**Group type**	**Order of group**	**Panel count**	**Significant merits**
Regular icosahedron	I_h ($\star$532)	120	20	Highest order of symmetry possible for triangular gridding
Overset icosahedron	T_h (3$\star$2)	24	20	
Regular octahedron*	O_h ($\star$432)	48	8	Permits the 'zinc-blende' staggered lattice, among others, that cannot be achieved in icosahedral geometry
Overset octahedron*	T_h (3$\star$2)	24	8	
Pellian sequence of hexagonal*/ dodecagonal dihedra	D_{6h} ($\star$226)	24	12, 96,180,1344,, $\ldots, \sigma_n S_{n+1}, \ldots$ $\sigma = 12(24)$ for odd(even) n.	All singularities confined to equator; approximately order-48 symmetry of D_{12h} for large n.
Regular tetrahedron**	T_d ($\star$332)	24	4	Domain unfolds into a single parallelogram
Hexagonal prism	D_{6h} ($\star$226)	24	36	Domain conveniently decomposes into six congruent parallegrams
Hexagonal antiprism	D_{6d} (2$\star$6)	24	48	Domain decomposes into a pair of congruent regular hexagons
Irregular octahedral Yin-Yang	D_{2d} (2$\star$2)	8	36	Domain decomposes into a pair of congruent irregular hexagons

to the group. In the ambiguous case of three mutually-orthogonal reflection planes, we choose the orientation which maximizes the rotational symmetry about the polar axis.

Unfortunately there seems to be no single universally-accepted notation for the space-groups we shall be concerned with. One traditional notation, much used in chemical spectroscopy, is the 'Schönflies notation' (for example, see Sharma 1982), which we shall primarily adopt but, in parentheses, we also indicate the newer 'orbifold notation' proposed originally by Thurston and developed and popularized in recent years by Conway and colleagues (Conway et al. 2001, 2003, 2008).

We are now ready to define the relevant groups by their generators. Although in many cases just two generators suffice, we shall try to provide (usually three) involutory generators (reflections and 180° gyrations) where possible since these can often be conveniently identified directly with the boundary segments (if reflections), or a fixed point on a boundary segment (if a gyration), of the fundamental region shown shaded in gray in each of the cartoons of Fig. 1. In cases where only one or two useful grid geometries share the group symmetry, we can provide the vertex, or vertices, that likewise generate the full complement of the polyhedron's vertices under the action of the group. All the groups described in this section are achiral (i.e., *not* chiral) since they contain reflections (for example, X and Y) amongst their symmetries.

The chiral restriction corresponding to each example is then the subgroup, of half the original order, comprising only the proper rotations.

(*a*) *Icosahedral group, I_h ($\star$532)*

The two sufficient generators are:

$$G_1 = X, \tag{3.3a}$$
$$G_2 = [-1/\phi, 1, 1/\phi^2]_{-2}, \tag{3.3b}$$
$$G_3 = Y. \tag{3.3c}$$

where ϕ is the 'golden number', $\phi = (\sqrt{5}+1)/2$. The order of this group is 120, making it the largest finite orthogonal group of three dimensional transformations. The 12 vertices of the icosahedron are generated by the single representative,

$$V = (1, 0, \phi)^{\mathsf{T}}, \tag{3.4}$$

which makes each equilateral triangular face have an edge of length two units.

Polyhedra with relatively high orders of symmetry tend not to fully preserve this symmetry when the spherically-mapped grid is modified by vertex oversets to remove from the map the metrical singularities; in the case of the triangular grid covering the regular icosahedron, the most symmetrical configuration of oversets (Fig. 1(e)) reduces the symmetry to the subgroup with 'pyritohedral' symmetry, to be described next.

The chiral restriction of the icsoahedral group is denoted I (532).

(*b*) *Pyritohedral group, T_h (3$\star$2)*

This group of order 24 is generated by,

$$G_1 = X, \tag{3.5a}$$
$$G_2 = [1, 1, 1]_{+3}, \tag{3.5b}$$

and is perhaps most familiarly exhibited by the pattern of gores on the surface of a standard volleyball ball. This is the only example we consider of a group that cannot be generated purely by involutions. Its Schönflies designation suggests a connection with the the tetrahedron and, in fact, the chiral restriction of this group is the chiral tetrahedral group, T (332).

(*c*) *Octahedral group, O_h ($\star$432)*

Three generators of this group of order 48 are the reflections:

$$G_1 = = X, \tag{3.6a}$$
$$G_2 = [1, -1, 0]_{-2}, \tag{3.6b}$$
$$G_3 = [0, 1, -1]_{-2}. \tag{3.6c}$$

The six vertices of the regular octahedron itself are generated by this group applied to the representative vertex,

$$V = (0, 0, \sqrt{2})^{\mathsf{T}}, \tag{3.7}$$

where, again, the sides of each triangular panel are each of length two units. The overset variant of the triangular-gridded octahedron breaks this symmetry; the most symmetrical configuration that includes vertex oversets has invariance with respect to the transformations of the pyritohedral group.

The cube also conforms to octahedral group symmetry. Its eight vertices are generated by:

$$V = (1/2, 1/2, 1/2)^{\mathsf{T}}, \tag{3.8}$$

giving square panels of unit sides.

The chiral restriction of the octahedral group is the group denoted O (432).

(*d*) *Tetrahedral group, T_d (⋆332)*

Three reflections,

$$G_1 = X, \tag{3.9a}$$
$$G_2 = Y, \tag{3.9b}$$
$$G_3 = [-1/\sqrt{2}, -1/\sqrt{2}, 1]_{-2}, \tag{3.9c}$$

define the tetrahedral group of order 24, which is also a subgroup of the octahedral group and of the icosahedral group. The four vertices of the tetrahedron itself are generated from

$$V = (0, 1, 1/\sqrt{2})^{\mathsf{T}}. \tag{3.10}$$

An overset version of the triangular tetrahedral grid would break the tetrahedral symmetry; the most symmetrical overset configuration would be one with the 'Yin-Yang' symmetry, D_{2d}, as illustrated in Fig. 1(k).

The chiral restriction of the tetrahedral group is denoted T (332).

(*e*) *'Yin-Yang' symmetry group, D_{2d} (2⋆2)*

The symmetry group of the various 'Yin-Yang' grids (Kageyama and Sato 2004) is exactly that of the tennis ball; it is an order-eight subgroup of the tetrahedral group generated by a reflection and a gyration:

$$G_1 = X, \tag{3.11a}$$
$$G_2 = [1, 1, 0]_2. \tag{3.11b}$$

By analogy with other antiprisms' symmetry groups (see below), this symmetry might be thought of as that of the antiprism of a degenerate two-sided polygon or 'edge', such as is generated by a stretching or compression along the Z-axis of the regular tetrahedron defined in the previous subsection. For the case of the square-griddable Yin-Yang configuration the parent polyhedron is the cube; it is then just the arrangement of the corner oversets that 'breaks' the cubic symmetry to that of the present less symmetrical group. But there are also triangular-griddable polyhedra with 12 vertices and possessing the Yin-Yang symmetry, of which the simplest decomposable into a surface made up of equilateral triangles is the highly

irregular convex polyhedron of four rectangles and four 'house-shaped' pentagons, and whose twelve vertices are generated by the action of the group on the inequivalent pair:

$$V_1 = (\sqrt{3}, \sqrt{3}, 1)^{\mathsf{T}}, \tag{3.12a}$$
$$V_2 = (\sqrt{3}, 0, 2)^{\mathsf{T}}. \tag{3.12b}$$

The surface is covered by 36 fundamental map panels.

Although the order-four chiral restriction of this group plays no part in any of the geometries we shall subsequently consider, we can state that its Schönflies and orbifold designations are D_2 (222).

(*f*) *Square antiprism group, D_{4d} (2⋆4)*

This order-16 group is, like all achiral antiprism groups, generated by a reflection and a gyration:

$$G_1 = X, \tag{3.13a}$$
$$G_2 = [\sqrt{2} - 1, 1, 0]_2, \tag{3.13b}$$
$$\tag{3.13c}$$

and is the first example of a group to which a nontrivial parameterized *family* or *type* of differently shaped grid geometries belongs. Generally, the surface of the antiprism divides naturally into a pair of (irregular) interlocking folded octagons, each separately exhibiting the symmetry of the dihedral planar group, D_4, of order eight. The example of a square-antiprism whose development divides into the smallest number (eight) of congruent square map panels obeying the vertex rules discussed in Section 1 actually has each 'octagon' of four panels forming a square, since the four vertices that lie at the corners of the northern square region alternate in longitude with the four vertices that lie at the midpoints of that square region's sides (which meet the corners of the corresponding southern square region). The half-shell of this particular antiprism is illustrated in Fig. 1(d). In order to construct the shape of the convex polyhedron associated with the generic square-antiprism we could apply the matrix representations of its group, D_{4d}, to a single representative vertex located at:

$$V = (1, 0, \zeta)^{\mathsf{T}} \tag{3.14}$$

for some shape-defining value, ζ, but in practice it is the shape of a representative sector of the developed map that is of more interest since the magnitude, ζ, plays no direct part in the construction of useful mappings to the sphere.

Generally, a member of the family of griddable square-antiprisms is specified uniquely by the pair, (a, b), of coprime integers, where a denotes the surface (radial) distance from the pole to a vertex parallel to a panel boundary in units of a panel side, while $\sqrt{2}b$ denotes the corresponding surface distance to a vertex in the direction at 45° to the panel sides. The total number of panels in such a mapping is $A = 8ab$. The simplest example, illustrated in Fig. 1(d), is of the specific type $(1, 1)$, with $A = 8$ as already stated.

The chiral restriction of this group is denoted D_4 (224).

(*g*) *Hexagonal antiprism group, D_{6d} (2⋆6)*

Continuing the antiprism pattern, the 24 elements of the group are generated by the two generators,

$$G_1 = X, \tag{3.15a}$$
$$G_2 = [2-\sqrt{3}, 1, 0]_2. \tag{3.15b}$$

Again, we are faced with an open-ended family of griddable polyhedra that share this symmetry group. Generically, the northern and southern regions are dodecagons that each conform to the planar hexagonal dihedral symmetry group, D_6, of order 12. A particular member of the family is specified uniquely by the positive integer pair, (a, b), with a denoting the radial map distance, in units of the elementary triangular map panel sides, between the pole and a vertex along a direction parallel to adjacent panel sides, while $\sqrt{3}b$ measures, in the same units, the distance from the pole to a vertex along the line at 30° to the adjacent panel sides. The surface is covered by $A = 24ab$ equilateral-triangular panels. In the simplest case, with specification $(a, b) = (1, 1)$ the dodecagons are in the shape of a 'star of David', while the next simplest case, with specification $(2, 1)$, has 'dodecagons' consisting of regular hexagons with half of the dodecagon's vertices lying at the midpoints of the hexagon's sides.

The chiral restriction of this group is denoted D_4 (224).

(*h*) *Edge prism or rectangular dihedron group, D_{2h} (⋆222)*

This order-eight group comprises the symmetries of a cuboid or of an 'edge prism' (rectangular dihedron) and is generated by the three Cartesian reflections,

$$G_1 = X, \tag{3.16a}$$
$$G_2 = Y, \tag{3.16b}$$
$$G_3 = Z. \tag{3.16c}$$

Restricting the group to its proper elements results in the subgroup D_2 (222).

(*i*) *Square prism group, D_{4h} (⋆224)*

Unlike the corresponding antiprism, the prism, in its standard presentation, is a figure that is symmetrical across the the equatorial plane. The square prism is generated by three reflections:

$$G_1 = X, \tag{3.17a}$$
$$G_2 = [1, -1, 0]_{-2}, \tag{3.17b}$$
$$G_3 = Z. \tag{3.17c}$$

Although the overset version of the cube that we call the 'barrel grid' has the original octahedral symmetry broken to this lower symmetry of order 16, the family of grids of greater interest with this symmetry are those associated with the various octagonal dihedra. In these grids, the vertex singularities lie on the equator but at longitudes of alternating spacing (in contrast, the antiprism grids have their vertices off the equator but at evenly spaced longitudes). Again,

the specification of a particular member of this family requires setting a pair of coprime integer parameters, (a, b), but the interpretation of a and b is different; a will denote the side of the hemispheric octagon in a direction parallel to square map panels and in units of the side of a map panel, while $\sqrt{2}b$ will denote the alternating sides at 45° to the panel sides. For the case where a is even, this dihedron shape admits an alternative gridding with half the number of panels, obtained by rotating the panel orientation by 45° and replacing (a, b) by the parameter pair $(b, a/2)$. Geometrical consistency constrains a and b by the inequalities, $a \geq 0$ and $b \geq 0$, with at least one of these parameters strictly positive. When one of them is zero, the dihedron becomes a square (degenerate 'octagon'). The simplest true octagon has the parameters, $(a, b) = (1, 1)$. The total map area, A, measured in map panels, is obtained by the formula:

$$A = 2a^2 + 8ab + 4b^2. \tag{3.18}$$

The chiral restriction of this group is D_4 (224).

(*j*) *Hexagonal prism group,* D_{6h} *(*⋆226*)*

Here the three generators of this group of order 24 can be chosen to be:

$$G_1 = X, \tag{3.19a}$$
$$G_2 = [1, -1/\sqrt{3}, 0]_{-2}, \tag{3.19b}$$
$$G_3 = Z. \tag{3.19c}$$

The dodecagonal dihedra form one family of griddable polyhedra with this symmetry. The poles must occupy only the corners of equilateral map panels. The shape of each dodecagonal hemisphere can be specified by the (positive integer) side parallel to panel boundaries, a, and the alternating oblique sides, $\sqrt{3}b$, in the same length units of panel sides. The smallest proper dodecagon is specified by parameter pair, $(a, b) = (1, 1)$. The number of equilateral triangular map panels in the whole surface is:

$$A = 12(a^2 + 4ab + 3b^2). \tag{3.20}$$

The other family of griddable polyhedra with this symmetry group comprises the hexagonal prisms themselves, of course. The aspect ratio in this case is specified by any positive integer pair, (a, b), where a measures the map distance from the pole to one of the vertices in the same hemisphere, while $\sqrt{3}b$ measures the map distance, in the same units, between each vertex and its opposite-hemisphere counterpart at the same longitude. While for *any* integer pair, (a, b), such a prism is always griddable by triangular panels of unit sides, note that when a is evenly divisible by 3, the surface is also griddable by panels larger (in linear dimensions) by $\sqrt{3}$ and rotated 30° with respect to the former orientation.

The chiral restriction of this group is denoted D_6 (226).

(*k*) *Discussion*

The group symmetries constrain the set of mappings in various ways. A reflection symmetry implies the existence of an invariant line (an axis of dihedral mirror symmetry) of the map, the points of which will always map to the same great circle on the sphere under *any* continuous

mapping that respects the symmetry. A proper rotation implies an antipodal pair of fixed points of the possible mappings, corresponding to the axis of rotation. Every line of intersection of pairs of reflection-symmetry planes is an axis of proper rotation, and therefore defines an antipodal pair of fixed points. We have already noted that each of our polyhedra possesses at least two reflection planes whose intersections have allowed us to fix the poles as invariant points of each symmetry group. Although the equator is *not* an invariant line of all the polyhedral mappings, a closer examination reveals that all our polyhedra possess additional invariant axes of proper rotation, including at least two that are orthogonally arranged around the equator, defining four fixed points there. The existence of fixed points of these mappings is what ensures the uniqueness of the systematic construction of Sections 5 and 6.

We have seen that all of the polyhedra discussed in this section, with the exception of the triangular-griddable Yin-Yang octahedron of Fig. 1(ℓ), share the property that all their vertices (and hence the convex polyhedron which forms the convex hull of these vertices) are generated by a single representative vertex through the action of the group. Another property shared by these eleven polyhedral types (but, again, not the Yin-Yang octahedron), is that, through each of these vertices, there passes a plane of reflection symmetry. The oversetting modification of the area-smoothed grids requires this symmetry to hold; the Yin-Yang octahedron is therefore excluded from this family of overset grids. There is an alternative oversetting procedure for modifying the unsmoothed conformal grids which does not require there to be a bilateral symmetry axis through each vertex, or require the oversetting incision to respect the symmetry if it exists; this alternative procedure is designed primarily to preserve the orthogonality of rectangular grids, but it also provides a way for the triangular-griddable Yin-Yang configuration to acquire its oversets (but without the option of smoothing the grid-areas prior to the oversetting).

While we seem to have laid out a profusion of possible polyhedral mapping geometries, there is obviously a question of which geometry is suitable for a given numerical formulation and modeling application. For a general global model where we are interested in accurately modeling every region equally, the least degree of map distortion is preferable – that is, the geometry with the highest degree of global symmetry. For a numerical formulation based on the conventional rectangular gridding, the spherical cubic geometry is the obvious choice. For a model based upon a triangular local grid (including finite volume models with hexagonal grid cells), without additional numerical restrictions, the icosahedron is then preferred. However, there are some *staggered* triangular grid arrangements in the horizontal, as well as three-dimensional staggerings, which *cannot* cover the polyhedral surfaces that contain vertices where the angle deficit is 60°. An example of an attractive three-dimensional staggered lattice is that of the 'zinc-blende' crystal structure which, in the modeling context, consists of a diamond lattice except with 'atoms' of wind having four 'atoms' of mass as tetrahedral neighbors and vice versa. For these grids to cover the sphere, it is necessary that any vertices have angular deficits of 120°. In such cases, the regular octahedron provides the most symmetrical global gridding. There is sometimes a concern that the presence of mapping singularities might cause numerical difficulties if they occur in the midlatitude baroclinically active zones. In these cases the dihedron geometries become attractive: octagonal dihedra for square grids; dodecagonal dihedra for triangular grids; hexagonal dihedron for the triangular grids with the 120° angular deficit restriction. There are also versions of the antiprism geometries with the symmetries D_{4d} and

D_{6d}, for square and triangular grids respectively, that can be found with their singularities *very* close to the equator; these grids have the advantage over their dihedron counterparts that their vertices are exactly equally-spaced in longitude. The triangular grid dihedra and antiprisms also enjoy a higher degree of zonal symmetry than the icosahedron (or octahedron) but, if high zonal symmetry is deemed especially important, a more uniform global distribution of the twelve singular points would be found amongst the family of hexagonal prisms.

The square dihedron and the regular tetrahedron share the dubious merit of being the only geometries we have considered here where the angular deficit is 180°. But this otherwise unattractively large angular distortion around each singularity (clearly visible in their depictions in Figs. 2(c) and (k)) might be of value for some numerical schemes. In the case of the conformal mappings, these two geometries are the only ones exhibiting integer power-law behavior around each vertex. The solutions can also both be expressed directly in terms of elliptic functions (Lee, 1976). Where these two geometries could be advantageous in practice is in comparing, under equitable conditions of mapping distortions, the relative merits of triangular-grid and square-grid numerics, since both geometries are continuously griddable by either rectangular or triangular lattices. The triangular gridding over the square dihedron cannot be *exactly* equilateral, just as the rectangular gridding over the tetrahedron cannot be *exactly* square. Nevertheless, using the 'Pell' rational approximations to $\sqrt{3}$ described in the next section, we can very closely approximate the intended ideals in both these respects.

Finally, we note that the Yin-Yang configurations enjoy the very convenient property that the global map splits tidily into two expansive uninterrupted congruent regions (rectangular in the case of the square-grid cube-based Yin-Yang, elongated hexagonal, in the case of the triangular-grid Yin-Yang configuration illustrated in Fig. 1(ℓ)).

4. Pell systems

In number theory, equations in integers:

$$Q^2 - kP^2 = \pm 1, \tag{4.1}$$

where positive k is not a squared number, are said to be of 'Pellian' form. For each such k there are always infinitely many possible solutions and they are connected by a characteristic recurrence that depends upon the k, allowing each Q/P to approximate $\sqrt{k}$ with diminishing error as the magnitudes of Q and P increase. The cases, $k = 2$ and $k = 3$, have particular geometrical significance owing to the fact that half-sides of regular octagons subtend angles at their centers of 22.5° with $\tan(22.5°) = \sqrt{2} - 1$ while half-sides of regular dodecagons subtend angles at their centers of 15° with $\tan(15°) = 2 - \sqrt{3}$.

Rational approximations to a square-root of an integer can be extracted from the successive 'convergents' of the continued fraction expansion of that square-root. The continued fraction,

$$f = q_0 + \frac{1}{q_1 + \frac{1}{q_2}},$$

is written as:

$$f = [q_0; q_1, q_2],$$

for example. For the expansion corresponding to the square-root of an integer, the sequence of q_i becomes cyclic. The Pell solutions Q_k and P_k can all be found, at the same cyclic intervals, as the numerators and denominators of convergents of such truncated approximations.

For the case, $k = 2$, the sequence of pairs (Q_n, P_n) are found to solve

$$Q_n^2 - 2P_n^2 = (-1)^n, \tag{4.2}$$

where $(Q_0, P_0) = (1, 0)$, $(Q_1, P_1) = (1, 1)$ and both Q_n and P_n obey the recurrence,

$$\psi_{n+1} = 2\psi_n + \psi_{n-1}. \tag{4.3}$$

The relevant continued fraction expansion for $\sqrt{2}$ is just,

$$\sqrt{2} = [1; 2, 2, 2, \ldots]. \tag{4.4}$$

TABLE 3. Pell sequences Q_n and P_n associated with $Q^2 - 2P^2 = \pm 1$, together with the corresponding continued fraction approximation to $1/\sqrt{2}$

n	Q_n	P_n	continued fraction	n	Q_n	P_n	continued fraction
0	1	0	$\frac{0}{1} = [0;]$	4	17	12	$\frac{12}{17} = [0; 1, 2, 2, 2]$
1	1	1	$\frac{1}{1} = [0; 1]$	5	41	29	$\frac{29}{41} = [0; 1, 2, 2, 2, 2]$
2	3	2	$\frac{2}{3} = [0; 1; 2]$	6	99	70	$\frac{70}{99} = [0; 1, 2, 2, 2, 2, 2]$
3	7	5	$\frac{5}{7} = [0; 1, 2, 2]$	7	239	169	$\frac{169}{239} = [0; 1, 2, 2, 2, 2, 2, 2]$

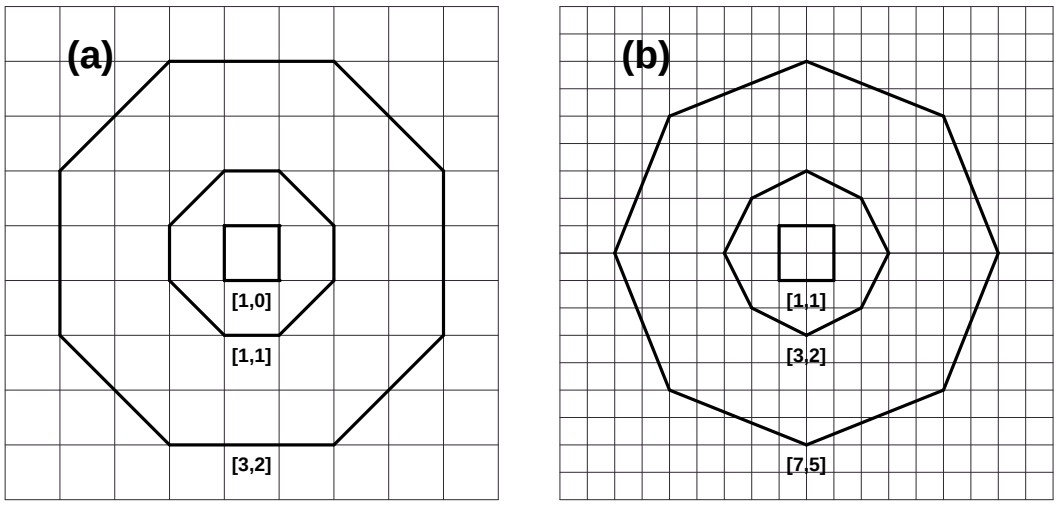

Figure 3. Two sequences of progressively more regular octagons associated with the Pellian sequences.

In Fig. 3 we see two ways of forming progressively more regular octagons on a square grid by employing the numbers from the two sequences associated with this Pell system. On the left, what we shall refer to as 'Type 1 octagons' have sides parallel and oblique to the panel sides, of $a_n = Q_n$ and $b_n = \sqrt{2}P_n$ units respectively. The corresponding area of the dihedral

surface of each such 'Pell octagon' is $A_n = 2Q_{2n+1}$ square panel units. The indexing convention here is chosen so that the case (a_0, b_0) in this sequence is the degenerate 'square dihedron'. The vertices are equidistant from the center but do not occur at regular angular intervals.

On the right is shown an alternative sequence of progressively more regular 'Type 2 octagons' drawn on the grid of panel boundaries. This time the vertices are not exactly equidistant from the center but they do at least occur at regular angular intervals of 45°. These vertices on the grid's principal axes occur at distances Q_{n+1} from the center, while the others are at distances $\sqrt{2}P_{n+1}$ in grid-panel units. The indexing convention is chosen, again, to make the degenerate case correspond to $n = 0$. The implied octagonal dihedra each have an area of $4P_{2n+2}$ square units. A tabulation of the first few P_n and Q_n and the corresponding continued fraction approximations to $1/\sqrt{2}$ is presented in Table 3.

For the case, $k = 3$, the sequence of pairs, (C_n, S_n), are found to solve

$$C_n^2 - 3S_n^2 = 1, \tag{4.5}$$

where $(C_0, S_0) = (1, 0)$, $(C_1, S_1) = (2, 1)$, and both C_n and S_n obey the recurrence,

$$\psi_{n+1} = 4\psi_n - \psi_{n-1}. \tag{4.6}$$

The relevant continued fraction expansion for $\sqrt{3}$ is,

$$\sqrt{3} = [1; 1, 2, 1, 2, \ldots], \tag{4.7}$$

with period-2 repeats. The tabulation of C_n and S_n, alternating with a related sequence-pair, T_n and D_n (for half-odd-integer n) is given in Table 4 together with the corresponding continued fraction expansion in the approximation to $1/\sqrt{3}$. The justification for the inclusion, and half-integer indexing, of the quantities T_n and D_n in Table 4 comes from observing that if we formally define the 'interpolated' quantities,

$$C_{n+1/2} = \frac{T_{n+1/2}}{\sqrt{2}}, \tag{4.8a}$$

$$S_{n+1/2} = \frac{D_{n+1/2}}{\sqrt{2}}, \tag{4.8b}$$

then, for both full-integer and half-integer indices, n, we would find that the following Pell-like recursions are satisfied:

$$C_{n+1/2} = \sqrt{2}C_n - C_{n-1/2}, \tag{4.9a}$$

$$S_{n+1/2} = \sqrt{2}S_n - S_{n-1/2}, \tag{4.9b}$$

and that now

$$C_n^2 - 3S_n^2 = (-1)^{2n}, \quad n = \frac{1}{2}, 1, \frac{3}{2}, \ldots, \tag{4.10}$$

which immediately gives us a larger range of ratios approximating $\sqrt{3}$ to choose from.

Figure 4 shows the two styles of Pell-based dodecagons analogous to the Type 1 and Type 2 octagons we showed in Fig. 3, except that now we find that the sequences derived from the

TABLE 4. Pell sequences C_n and S_n obeying $C^2 - 3S^2 = 1$, the related sequences, T_n and D_n obeying $T^2 - 3D^2 = -2$, and the corresponding continued fraction approximation to $1/\sqrt{3}$.

n	C_n	S_n	T_n	D_n	continued fraction
0	1	0			$\frac{0}{1} = [0;\,]$
$\frac{1}{2}$			1	1	$\frac{1}{1} = [0;\,1]$
1	2	1			$\frac{1}{2} = [0;\,1,\,1]$
$\frac{3}{2}$			5	3	$\frac{3}{5} = [0;\,1,\,1,\,2]$
2	7	4			$\frac{4}{7} = [0;\,1,\,1,\,2,\,1]$
$\frac{5}{2}$			19	11	$\frac{11}{19} = [0;\,1,\,1,\,2,\,1,\,2]$
3	26	15			$\frac{15}{26} = [0;\,1,\,1,\,2,\,1,\,2,\,1]$
$\frac{7}{2}$			71	41	$\frac{41}{71} = [0;\,1,\,1,\,2,\,1,\,2,\,1,\,2]$
4	97	56			$\frac{56}{97} = [0;\,1,\,1,\,2,\,1,\,2,\,1,\,2,\,1]$
$\frac{9}{2}$			265	153	$\frac{153}{265} = [0;\,1,\,1,\,2,\,1,\,2,\,1,\,2,\,1,\,2]$
5	362	209			$\frac{209}{362} = [0;\,1,\,1,\,2,\,1,\,2,\,1,\,2,\,1,\,2,\,1]$
$\frac{11}{2}$			989	571	$\frac{571}{989} = [0;\,1,\,1,\,2,\,1,\,2,\,1,\,2,\,1,\,2,\,1,\,2]$

C and S sequences (shown in red) interleave with those derived from the T and D sequences (shown in blue). The integer aspect parameters (a, b) are interpreted, as before, as the lengths of alternating sides of the Type-1 polygon parallel and oblique to the panel alignment. In the present case, the panels are equilateral triangles whose sides define the 'unit' of distance. By this measure, the Type-1 dodecagon's sides are respectively a, and $\sqrt{3}b$, units parallel and oblique to panel sides. Again, for the Type-2 polygon series, a measures radial map distance from the polygon's center to the vertices in the direction parallel to panels sides, $\sqrt{3}b$ measures distance to those in the oblique directions. It is convenient to index the Pellian dodecagons of Type 1, starting from $n = 0$ (the hexagonal case), so that their aspect parameters are:

$$(a_n, b_n) = \begin{cases} (C_{n/2}, S_{n/2}) & : \quad n \text{ even} \\ (T_{n/2}, D_{n/2}) & : \quad n \text{ odd}, \end{cases} \tag{4.11}$$

and the areas (in map panels) of the corresponding dodecagonal dihedra then become:

$$A_n = \begin{cases} 12S_{n+1} & : \quad n \text{ even} \\ 24S_{n+1} & : \quad n \text{ odd}. \end{cases} \tag{4.12}$$

For Type 2 dodecagons illustrated in panel (b), it is more convenient to begin the indexing of the Pellian cases from $n = 1$ since, in this family there are no degenerate polygons. Thus, the indexed parameter pairs, (a_n, b_n) are defined:

$$(a_n, b_n) = \begin{cases} (T_{n/2}, D_{n/2}) & : \quad n \text{ odd} \\ (C_{n/2}, S_{n/2}) & : \quad n \text{ even} \end{cases} \tag{4.13}$$

and the areas (in map panels) for the corresponding hexagonal antiprisms are:

$$A_n = \begin{cases} 24S_n & : \quad n \text{ odd} \\ 12S_n & : \quad n \text{ even}. \end{cases} \tag{4.14}$$

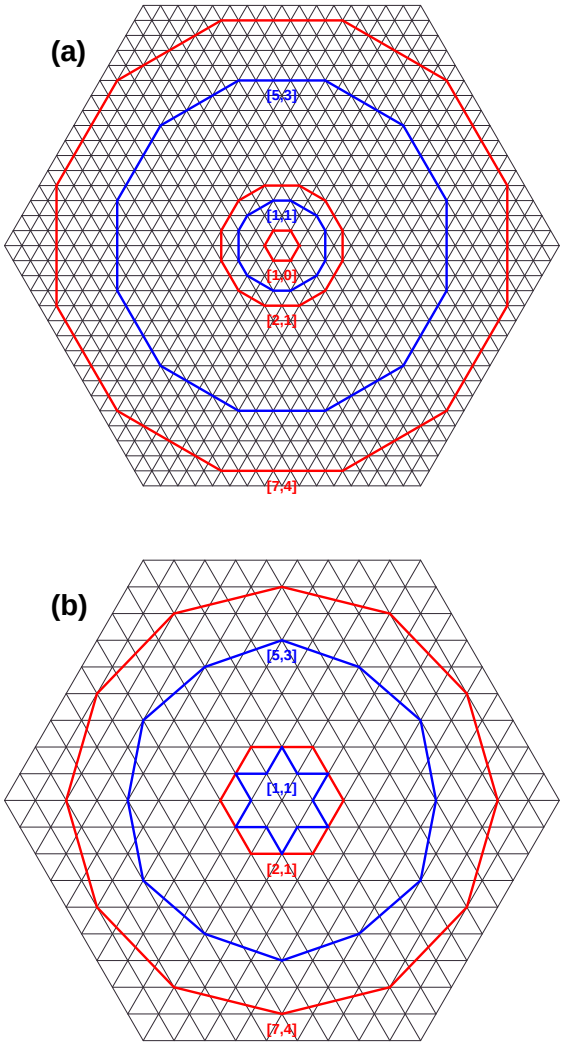

Figure 4. Two sequences of progressively more regular dodecagons associated with the Pellian sequences.

By choosing members of these Pellian families for the dihedra and for the antiprisms, we ensure that the polygonal half-domains, in each case, are as near to being regular polygons as is possible for the given allowance of map panels. The other family of polyhedra whose aspect parameters might advantageously be taken from the Pell pairs, (C_n, S_n) or (T_n, D_n), are the hexagonal prisms; in this case, the choice of a Pell pair for the parameters (a, b) ensures that the side faces of the prism are as close as possible to being square, if this is deemed desirable.

5. Continuous symmetrical polyhedral mappings to the sphere

Of all the continuous polyhedral mappings from the surface of the given polyhedron to the surface of the sphere performed in such a way that the polyhedron's symmetries are preserved,

the conformal mapping is distinguished by being, in some sense the 'smoothest' mapping possible. Without the constraint of symmetry the conformal mapping solutions for any particular polygon form a six-real-parameter continuous family related to one another through Möbius transformations. A Möbius transformation is most easily described by its action on a point of the sphere represented by that point's polar stereographic image, z, in the complex plane, where $z = 0$ denotes the pole antipodal to the projection center and the unit circle, $|z| = 1$, is the image of the equator. Then the general Möbius transformation from one point on the sphere, represented by z, to another, represented by z', takes the form:

$$z' = \frac{az + b}{cz + d}, \tag{5.1}$$

where $ad - bc \neq 0$. Since a change of the complex parameters, $a' = wa$, $b' = wb$, $c' = wc$, $d' = wd$ for any complex scaling factor, w, leaves the transformation unchanged, the (real) dimensionality of this kind of transformation is six (not eight). Transformations of this kind were proposed by Schmidt (1977) as a way to provide enhanced resolution in a single region of interest, but preserving the global model structure. For spectral models this is a particularly useful device and is used by MeteoFrance's Arpège model (Courtier and Geleyn 1988). If the images of any three distinct points undergoing a Möbius transformation are given, then the Möbius transformation itself is uniquely specified. As we stated in Section 3, all of our griddable polyhedra possess at least six fixed points (the two poles plus at least four points spaced 90° apart around the equator), which is more than enough to guarantee that the *symmetrical* conformal mapping from each surface to the sphere is unique.

The symmetrical conformal mapping solution provides the basis of all the grid constructions we shall consider.

(*a*) *Constructing a symmetrical conformal mapping*

The defining equations of a conformal mapping are the Cauchy-Riemann (C-R) equations. Although they are most familiarly written in the context of planar maps, we can adapt them to the case of a mapping between two-dimensional Cartesian 'map coordinates', $\mathbf{x} = (x, y)$, and the three-dimensional Earth-centered Cartesian position vector, $\mathbf{X}$, for the spherical Earth of unit radius. In association with the normalization constraint, the spherical C-R equations become:

$$\mathbf{X}\cdot\mathbf{X} = 1, \tag{5.2a}$$

$$\frac{\partial \mathbf{X}}{\partial x} = \frac{\partial \mathbf{X}}{\partial y}\times\mathbf{X}, \tag{5.2b}$$

but in this form they are numerically inconvenient to apply. It is more convenient to reformulate these equations as an equivalent variational principle. We do this by minimizing the integral of the dot-product of the residual vector of (5.2b) with itself, subject to the constraint of (5.2a). This constrained minimum occurs when, and only when, the residual becomes the null vector everywhere. Thus, we first expand (using the normalization condition and its derivative):

$$\begin{aligned} L(\mathbf{x}) &= \left(\frac{\partial \mathbf{X}}{\partial x} - \frac{\partial \mathbf{X}}{\partial y}\times\mathbf{X}\right)\cdot\left(\frac{\partial \mathbf{X}}{\partial x} - \frac{\partial \mathbf{X}}{\partial y}\times\mathbf{X}\right) \\ &= \frac{\partial \mathbf{X}}{\partial x}\cdot\frac{\partial \mathbf{X}}{\partial x} + \frac{\partial \mathbf{X}}{\partial y}\cdot\frac{\partial \mathbf{X}}{\partial y} - 2\left(\frac{\partial \mathbf{X}}{\partial x}\times\frac{\partial \mathbf{X}}{\partial y}\right)\cdot\mathbf{X}. \end{aligned} \tag{5.3}$$

We notice that,

$$\Delta(x,y) = \left(\frac{\partial \mathbf{X}}{\partial x} \times \frac{\partial \mathbf{X}}{\partial y}\right) \cdot \mathbf{X}, \tag{5.4}$$

is just the mapping Jacobian, dA/da, where dA denotes the infinitesimal element of solid angle, or area of on unit sphere, while $da = dx\, dy$ denotes the element of map-domain area. Thus,

$$\int \Delta(\mathbf{x}) da = \mathcal{A} = 4\pi, \tag{5.5}$$

regardless of the mapping solution, $\mathbf{X}(\mathbf{x})$, provided it covers the unit sphere as a single-valued continuous vector function. Therefore this term can be omitted from the variational integral without changing the solution. Thus, introducing a Lagrangian multiplier scalar function, $\Lambda(\mathbf{x})$ associated with the constraint, (5.2a), we can write

$$\begin{aligned} 2\mathcal{L} &= 2\mathcal{A} + \int L(\mathbf{x}) + (\mathbf{X}\cdot\mathbf{X} - 1)\Lambda(\mathbf{x})\, da \\ &= \int \frac{\partial \mathbf{X}}{\partial x}\cdot\frac{\partial \mathbf{X}}{\partial x} + \frac{\partial \mathbf{X}}{\partial y}\cdot\frac{\partial \mathbf{X}}{\partial y} + (\mathbf{X}\cdot\mathbf{X} - 1)\Lambda(\mathbf{x})\, da. \end{aligned} \tag{5.6}$$

This variational principle was asserted by Purser and Rančić (1998) for the general conformal solution, and generalized through the inclusion of additional terms designed to reduce the areal disparities of the implied grid cells. (Since we are adopting an alternative mechanism for achieving a qualitatively similar result in the next subsection, we shall be not concerned with that generalization here. Other variational methods for general computational grid generation problems are described in Thompson et al., 1985.)

The Euler-Lagrange equations resulting from stationary variations $\delta\mathcal{L} = 0$ associated with arbitrary variations of $\Lambda(x,y)$ and $\mathbf{X}(x,y)$ respectively give us the conformal mapping conditions equivalent to (5.2a) and (5.2b), but now in the much more convenient form of the self-adjoint vector elliptic system:

$$\frac{\partial^2 \mathbf{X}}{\partial x^2} + \frac{\partial^2 \mathbf{X}}{\partial y^2} = \mathbf{X}\Lambda. \tag{5.7}$$

constrained by (5.2a).

The solution of the conformal mapping need not be carried out explicitly for the entire polyhedron – just a representative connected 'minimal fundamental region' which, through the action of the symmetry group, generates congruent images covering the entire sphere. For example, for the cube or the square dihedron, the minimal fundamental region is the 45° right-angle triangle forming one octant of a square face, bounded by three of the polyhedron's reflection-symmetry planes.

The multigrid method provides probably the most suitable practical method of solving the conformal mapping problem for generic polyhedral geometries. Rančić et al. (1996), and Purser and Rančić (1997), provide alternative extremely accurate Fourier-transform-based methods for the cube and octahedral dihedron geometries, which can also be adapted to other polyhedra. But since we shall be needing to use a similar multigrid structure in order to tackle the problem of achieving more equitable mapping Jacobians, it is natural to use this versatile approach for *all* stages of the grid construction.

The idea underlying the multigrid method is to remove the residual errors, at a given scale, in the interim solution to the elliptic problem on a grid whose scale of resolution is comparable to that of the targetted residual; the remaining residual, which is recalculated, is then projected onto a coarser grid and the process continued recursively. At the coarsest scale, the residual is removed completely and rapidly, either by iterations or by direct solution, since the problem size at this scale is small enough. The corrections are then progressively interpolated back down to finer scales and the cycle of relaxation iterations is carried out again to achieve a further level of error reduction, and so on until convergence is achieved. The situation is depicted schematically in Fig. 5.

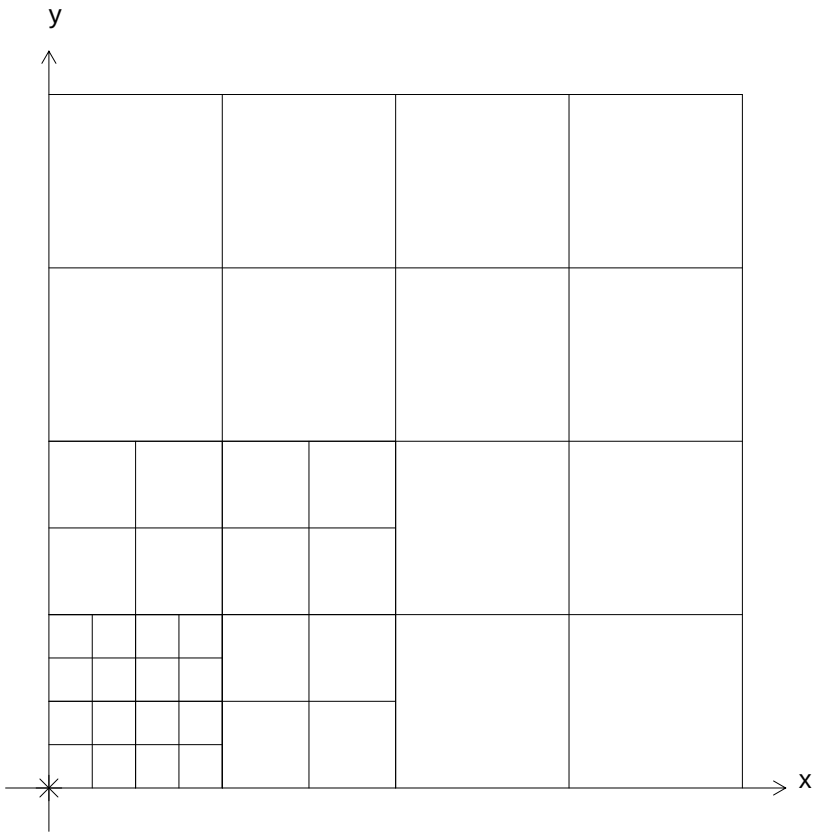

Figure 5. Schematic depiction of the telescoping multigrid structure around map singularity marked by the asterisk. Involutory symmetries that have the singularity as a fixed point imply that it is generally not necessary to completely surround the singularity with grid points; in this depiction one corner of one panel of a square grid is depicted, as might be seen in the cubic or square-dihedron geometries.

In a case such as we have in these polyhedral mapping constructions, we have the additional problem of the coordinate singularities to consider. Here also, the multigrid framework provides a natural solution by allowing a succession of progressively finer nested grids to 'telescope' towards the singularity without being required to cover the whole of the solution domain. Thus, if solving for the $\mathbf{X}(x, y)$ of the fundamental region of the cube, the telescoping portions of the sequence cover progressively smaller triangular regions converging on the corner singularity. The numerical finite-difference elliptic operator need only be applied to the outer 75%, where

the solution is expected to be relatively smooth, whenever there is known to be a finer-resolving grid-sequence that can take care of the innermost 25% at this stage. In this way, the problem of accurately approximating the elliptic operator in the neighborhood of the singularity is deferred until the telescoping grid has become sufficiently fine that the known asymptotic power law form of the solution, adjusted only by an estimated constant scaling factor, can be substituted in place of the problematic numerical finite-difference evaluation in the corner region of the finest grid.

(*b*) *A smooth generalization of the conformal maps that homogenizes the Jacobian*

We use each polyhderon's conformal solution as the starting point for a parameterized continuous spectrum of more homogeneous mappings with the same symmetry. The parameter, τ, ranges between zero at the conformal extreme of this spectrum, to unity at the other extreme where the mapping Jacobian, $\Delta(\mathbf{x}, \tau)$, becomes perfectly uniform. We envisage this τ to be a time-like parameter and, according to this view, the 'flow' of mapping image vectors, $\mathbf{X}(\mathbf{x}, \tau)$, is characterized by an irrotational divergent 'velocity', $\mathbf{V}(\mathbf{x}, \tau) = \partial \mathbf{X}(\mathbf{x}, \tau)/\partial\tau$, which can therefore be identified with the gradient of an appropriate velocity potential, $\chi(\mathbf{x}, \tau)$.

In order to be sure of avoiding complications that can arise should the total map-area,

$$a = \int da = \int \int dx\, dy \tag{5.8}$$

not be dimensionless, it is convenient to rescale and nondimensionalize this Jacobian,

$$\hat{\Delta}(\mathbf{x}, \tau) = \frac{a}{4\pi}\Delta(\mathbf{x}, \tau), \tag{5.9}$$

which must satisfy,

$$\int \hat{\Delta}(\mathbf{x}, \tau)\, da = a, \tag{5.10}$$

for all τ, and tend continuously to $\hat{\Delta}(\mathbf{x}, 1) = 1$ as $\tau \to 1$. Then

$$D(\mathbf{x}, \tau) = \frac{\partial}{\partial\tau} \ln \hat{\Delta}(\mathbf{x}, \tau), \tag{5.11}$$

provides a natural kinematic definition of the 'divergence' which must itself satisfy the integral consistency condition:

$$\int \hat{\Delta}(\mathbf{x}, \tau) D(\mathbf{x}, \tau)\, da = 0. \tag{5.12}$$

The simplest consistent prescription for this divergence,

$$D(\mathbf{x}, \tau) = D'(\tau) - \ln \hat{\Delta}(\mathbf{x}, 0), \tag{5.13}$$

can be integrated as an ordinary differential equation for each separate $\mathbf{x}$ to show that,

$$\hat{\Delta}(\mathbf{x}, \tau) = F(\tau) \left(\hat{\Delta}(\mathbf{x}, 0)\right)^{1-\tau}, \tag{5.14}$$

does indeed evolve continuously towards unity at $\tau = 1$. The normalizing factor needed to maintain (5.10) is given by:

$$F(\tau) = \frac{a}{\int \left(\hat{\Delta}(\mathbf{x}, 0)\right)^{1-\tau} da}, \tag{5.15}$$

and is related to $D'(\tau)$ of (5.13) through

$$D'(\tau) = \frac{d \ln(F(\tau))}{d\tau} = \frac{\int \ln[\hat{\Delta}(\mathbf{x}, 0)] \hat{\Delta}(\mathbf{x}, \tau)\, da}{a}. \tag{5.16}$$

Note that

$$F(0) = F(1) = 1. \tag{5.17}$$

The Poisson equation that connects our known divergence field, $D(\mathbf{x}, \tau)$, to its corresponding velocity potential, $\chi(\mathbf{x}, \tau)$, needs to be expressed in map coordinates. This is most easily done by adopting full tensor notation (e.g., Kreysig 1991, Synge and Schild 1949) with upper indices denoting contravariant components, lower indices denoting covariant components, and an implied summation running over any paired upper and lower indices in any term. For the present, we need only be concerned with the **X**-space covariant metric tensor, G_{ab}, on the unit sphere, where its components can be taken to form an identity matrix, $G_{ab} = \delta_{ab}$ in order to yield the correct infinitesimal distance, ds, on the surface,

$$ds^2 = G_{ab} dX^a\, dX^b. \tag{5.18}$$

(Although the components perpendicular to the surface seem already redundant, they do no harm and it will actually be convenient to further generalize this metric *off* the sphere in Section 6 when we use geodesics to construct the oversets of the various grids.) The Jacobian operator connecting the coordinate systems is:

$$J_i^a = \frac{\partial X^a}{\partial x^i}, \tag{5.19}$$

where now superscripts are to be interpreted as components, $x^1 \equiv x$ and $x^2 \equiv y$, not exponents. The **x**-space covariant metric tensor, g_{ij}, while *not* so trivial, is still easily obtained from the Jacobian operator:

$$g_{ij} = G_{ab} J_i^a J_j^b, \tag{5.20}$$

which inverts to give the contravariant representation of the metric, g^{ij}. These map-space metrics are functions of both $\mathbf{x}$ and τ, of course. Thus, in **x**-coordinates, the contravariant velocity vector is given from the as-yet unknown velocity potential via:

$$v^i(\mathbf{x}, \tau) = g^{ij}(\mathbf{x}, \tau) \frac{\partial \chi(\mathbf{x}, \tau)}{\partial x^j}. \tag{5.21}$$

The scalar mapping Jacobian, Δ, is equivalently the square-root of the determinant of the representation g_{ij}. It, or else its rescaled counterpart, $\hat{\Delta}$, is needed to express the divergence of the velocity in consistent tensorial form. Thus, by writing,

$$D(\mathbf{x}, \tau) = \frac{1}{\hat{\Delta}(\mathbf{x}, \tau)} \frac{\partial}{\partial x^i} \hat{\Delta}(\mathbf{x}, \tau) v^i, \tag{5.22}$$

and substituting (5.21) we obtain the self-adjoint elliptic equation for χ that we need to solve at each τ in order to advance the integration of the map-migration flow field. For clarity, we omit the explicit dependence upon $\mathbf{x}$ and τ in the following equation, but note that *every* factor of it does have this dependency:

$$\frac{1}{\hat{\Delta}}\frac{\partial}{\partial x^i}\hat{\Delta}g^{ij}\frac{\partial\chi}{\partial x^j} = D. \tag{5.23}$$

From the v^i given by (5.21) we immediately obtain:

$$\frac{\partial X^a}{\partial\tau} \equiv V^a = J^a_i v^i, \tag{5.24}$$

which allows us to advance the numerical integration of $\mathbf{X}$ towards a more homogeneous mapping.

At no point does the evolution prescribed above deviate from the symmetries of the original polyhedron. By stopping at some predetermined vaue of τ we have precise control over the degree of residual Jacobian-inhomogeneity we are prepared to tolerate. As with the conformal mapping construction, we can fully exploit the symmetry by solving the equations only with a gridded fundamental region much smaller than the entire spherical domain, and we can use the multigrid approach, including the telescoping of ever-finer grids surrounding the singularity, to minimize the spatial truncation error. The truncation error in τ can be reduced by an appropriate combination of small numerical steps, $\Delta\tau$, and the adoption of a high-order 'time'-integration scheme.

One very important and distinguishing feature of the new approach to systematically homogenizing the mapping Jacobian in this way is that, like the starting conformal solution, the finite-τ members of the family preserve a tractable asymptotic scaling of the solution around the singularities. The dominant part of this scaling can be characterized *exactly* in power-law terms dependent (apart from trivial scaling) only upon the angular deficit of the original polyhedron. This does not seem to be a property shared by the variational area-smoothing procedures proposed by Purser and Rančić (1998) and by Tomita et al. (2002). However, it is numerically advantageous as it means that this accurate asymptotic solution can be substituted for an unreliable and inaccurate finite-difference evaluation in the immediate vicinity of the singularity at the finest level of the telescoping multigrid solvers, both in the construction of the original conformal mapping solution, and in any stage of the finite-τ generalization of it. The accuracy of those respective solutions is never compromised by having the elliptic operators' differencing stencils intersecting the singularity. This is because, at any level of the telescoping multigrid hierarchy, if there is a grid point where the vertex interferes with the elliptic operator's stencil centered on that grid point, the solution-relaxation there is only used to accelerate the residual reduction deriving either from a finer-grid diagnostic (where the grid point at the same location is out of range of direct interference), or from the extremely accurate asymptotic solution directly (only when the point is very close to the singularity). Metaphorically, the asymptotic solution around the singularity serves as the 'keystone' guaranteeing the integrity of the multigrid solution at every interdependent member of the telescoping sequence of grids. Recognizing its importance, we devote the following subsection to an analysis of this asymptotic behavior.

(*c*) *Asymptotic scaling near a vertex*

At $\tau = 1$ a configuration is obtained that satisfies the desideratum of areal uniformity exactly since, at this time, $\Delta(\mathbf{x}, 1)$ is constant and the mapping is of the perfectly equal-area type. But each intermediate τ is also associated to a particular grid configuration which, while still possessing singular behavior at each vertex, has a scaling about this vertex which is characteristic of the parameter τ and of the initial scaling (at $\tau = 0$). The process is begun from the conformal solution, whose scaling is already predictable according to the angle-deficit at this vertex. If the angle deficit in radians is $2\pi\gamma$, then the scaling of the true radial distance $R(r, 0)$ from the singularity with respect to the conformal map's radial distance, $r = (x^2 + y^2)^{1/2}$, takes the form:

$$R(r, 0) \approx K(0) r^{p(0)}, \tag{5.25}$$

for some constant, $K(0)$, that must be obtained by examination of the particular conformal mapping solution, and the positive exponent, $p(0)$, that depends purely on the angular deficit by:

$$p(0) = \frac{1}{1 - \gamma}. \tag{5.26}$$

For example, for a cube with angle deficit $\gamma = 1/4$ the scaling near the vertex for the conformal case is:

$$R(r, 0) \propto r^{4/3}, \tag{5.27}$$

while for the icosahedron, with $\gamma = 1/6$ it is:

$$R(r, 0) \propto r^{6/5}. \tag{5.28}$$

At intermediate stages of the migration process, the progressively weakening singularity, seen at a distance close enough to the singularity for the anisotropic effects of the divergent advecting field to be negligible, scales like:

$$R(r, \tau) \approx K(\tau) r^{p(\tau)}, \tag{5.29}$$

for some scaling coefficient, K, and some exponent, p, which both depend only upon τ. Factoring in the angular deficit for the map domain around the singularity at $r = 0$ we deduce that the Jacobian, Δ, in this vicinity behaves asymptotically for $r \to 0$:

$$\Delta(r, \tau) \approx \frac{1}{1 - \gamma} \frac{R}{r} \frac{\partial R}{\partial r} = p(0) p(\tau) K^2(\tau) r^{(2p(\tau) - 2)}, \tag{5.30}$$

and its logarithm:

$$\ln \Delta(r, \tau) \approx \ln(p(0)p(\tau)) + \ln K^2(\tau) + (2p(\tau) - 2) \ln r. \tag{5.31}$$

Recalling the kinematic definition of divergence, (5.11), we obtain:

$$D(r, \tau) \approx \frac{d}{d\tau} \left(\ln(p(0)p(\tau)) + \ln K^2(\tau) \right) + 2 \frac{dp(\tau)}{d\tau} \ln r, \tag{5.32}$$

which must match the asymptotic form of the prescription, (5.13). Using (5.16) this may be expressed:

$$D(r, \tau) \approx \frac{d \ln F(\tau)}{d\tau} + \ln \left(\frac{4\pi}{a} \right) - \ln p^2(0) - \ln K^2(0) - \frac{2\gamma}{1 - \gamma} \ln r. \tag{5.33}$$

Matching coefficients for the dominant term, $\ln r$, we find:

$$\frac{dp(\tau)}{d\tau} = -\frac{\gamma}{1-\gamma}, \tag{5.34}$$

which, with (5.26), implies:

$$p(\tau) = \frac{1-\tau\gamma}{1-\gamma}. \tag{5.35}$$

Matching the remaining terms independent of r:

$$\frac{d}{d\tau}\left(\ln K^2(\tau) + \ln(p(0)p(\tau)) - \ln F(\tau)\right) = -\ln p^2(0) - \ln K^2(0) + \ln\left(\frac{4\pi}{a}\right). \tag{5.36}$$

Thus,

$$\ln K^2(\tau) + \ln(p(0)p(\tau)) - \ln F(\tau) = C + \tau\left[-\ln p^2(0) - \ln K^2(0) + \ln\left(\frac{4\pi}{a}\right)\right], \tag{5.37}$$

where the integration constant, C, is isolated by setting $\tau = 0$:

$$C = \ln p^2(0) + \ln K^2(0), \tag{5.38}$$

whence,

$$K^2(\tau) = \frac{p(0)}{p(\tau)} F(\tau) K^2(0) \left(\frac{4\pi}{a p^2(0) K^2(0)}\right)^{\tau}. \tag{5.39}$$

For the uniform-Jacobian solution,

$$K^2(1) = \frac{4\pi p(0)}{a} = \frac{4\pi(1-\gamma)}{a}. \tag{5.40}$$

If, for example, numerical methods are perfected for the spherical cube geometry associated with some values of τ, the same methods should work well on any of the spherical 'octagons' (Purser and Rančić, 1998) constructed with the *same* parameter τ, since the angle deficits, and hence the scalings near the singularities of the conformal cube and octagons, are identical.

The time-dependent migrating velocity field, $\mathbf{V}$, may or may not vanish at each vertex depending upon whether the symmetry group implies the vertex to be a fixed point. The vertices of only Figs. 1(a), (c), (e), (f), and (k), have this property. In the other cases illustrated, the velocity may translate the vertex itself. Nevertheless, if we redefine the $\mathbf{V}$ locally to represent velocity relative to that of the vertex, then the scaling of this relative velocity sufficiently close to the vertex will tend to be dominated by the singular portion of the purely radial component. In order to study the scaling of this advecting 'migration flow', whose azimuthally-averaged radial component will be denoted V, we shall need to express the approximate divergence operator applied to this velocity near $r = 0$:

$$D \approx \frac{1}{R}\frac{\partial}{\partial R} RV \approx \frac{1}{pKr^{(2p-1)}}\frac{\partial}{\partial r} r^p V. \tag{5.41}$$

But we know from (5.16) and (5.33) that the asymptotic form of the divergence at $r \to 0$ has the dominant term:

$$D(r, \tau) \approx -\frac{2\gamma}{1-\gamma} \ln r, \tag{5.42}$$

Integration gives $V(r, \tau)$ directly:

$$V(r, \tau) \approx -\frac{\gamma}{1-\gamma} K(\tau) r^{p(\tau)} \ln r, \tag{5.43}$$

or briefly:

$$V \approx -\frac{\dot{p}}{p} R \ln (R/K) , \tag{5.44}$$

where,

$$\dot{p} \equiv \frac{dp}{d\tau}. \tag{5.45}$$

We relate this asymptotic approximation, V, to the radial gradient of a velocity potential χ, which is approximately a function of r or of R locally:

$$V \approx \frac{\partial \chi}{\partial R} \approx \frac{1}{pKr^{(p-1)}} \frac{\partial \chi}{\partial r}. \tag{5.46}$$

Since we know from Section 3 that all vertices are equivalent with respect to the symmetries of the polyhedron's group (except for the polyhedron of Fig.1(ℓ) to which it is inappropriate to apply this area-homogenization in any case), it is consistent to adopt the convention that χ vanishes at each vertex. Again, by a direct integration we find that:

$$\chi(r, \tau) \approx -\left(\frac{\gamma}{1-\gamma}\right) \frac{K^2(\tau) r^{2p(\tau)}}{2} \ln r, \tag{5.47}$$

or briefly:

$$\chi \approx -\frac{\dot{p}}{p} \frac{R^2}{2} \ln (R/K) . \tag{5.48}$$

With the assumption that the telescoping multigrid's innermost and finest grid domain fits, in its entirety, within a tiny radius of the singularity where the asymptotic solutions for both $\mathbf{X}(\mathbf{x}, \tau)$ (deduced from $R(r, \tau)$ assuming local isotropy) and χ are extremely accurate approximations, we substitute them as alternatives to finite difference-derived solutions. Thus, we avoid ever having to rely on the accuracy of such finite differences anywhere near the coordinate singularity in both the elliptic system for the conformal solution and, where applicable, in the evolving series of solutions for $\chi(\tau)$.

6. Overset modifications of the smoothed grids

This section considers the problem of removing the remaining numerical defects associated with the grid singularities. A procedure is proposed here, valid for all but one of the grids we have considered, that preserves the perfect continuity and smoothness of these grids across at least those central portions of the edges between the square or triangular map panels that

are not in the immediate vicinity of the original map singularies. But we recognize that, near the singularities themselves, the only successful remedy involves some judicious grid surgery, followed by a local stretching applied at both sides of each incision, in order to restore to each piece a more natural corner angle. Each incision always runs out from the vertex along a pair of edges between map panels and, collectively, the orientations of these cuts is chosen to maximize the order of the group of orthogonal symmetries of the configuration as it is modified by such cuts. The choice is clearly not always unique, but examples conforming to this principle are depicted in Fig. 1 by the bold segments radiating from each of the angle-deficient vertices that are visible on these half-shells. The configuration of cuts is also assumed to remain mirror-symmetric about the plane dividing the half-shell from its complement. The two actual (geographical) vertex angles formed by these angled cuts sum to 360°, requiring either that both are 180°there, or that one of them exceeds this amount. The natural grid angles, however, never exceed 180°and are never *both* this amount either. The remaining singular feature of the smoothed grids is their pronounced and unbounded curvature around these offending vertices; it is this feature that is remedied by a stretching of the two locally separated sides of the grid into an overlapping configuration, restoring angles on each side that have their natural locally convex shape.

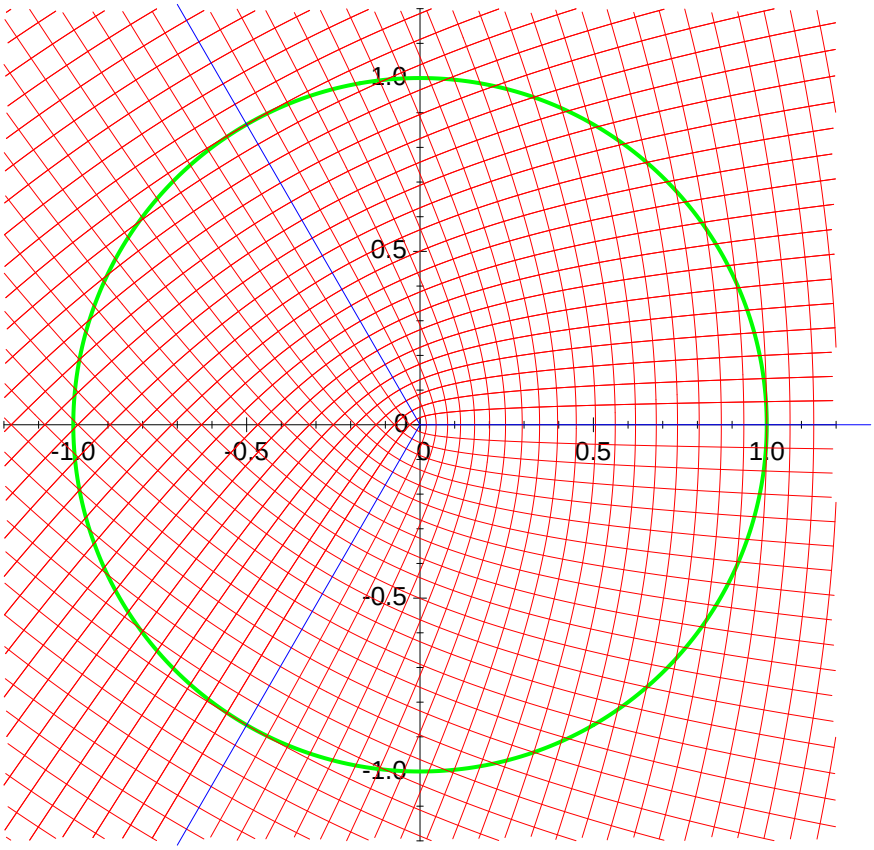

Figure 6. A portion of the conformal cubic grid showing a disc within which the grid will be divided into two discontinuous pieces and reconstructed to remove the central singularity.

For some of the grids shown in Fig. 1 the overall symmetry is not altered by the introduction of these incisions and the overlapping that follows. But, for the highly symmetric polyhedra of panels (a) (the cube), (e) (the icosahedron), (f) (the regular octahedron), and (k) (the regular tetrahedron), the inclusion of cuts necessarily results in a lowering of their symmetries. The symmetry characteristics of these original and modified polyhedral grids are summarized in Tables 1 and 2. It is also noteworthy that, for all the configurations with angle-deficits of $\gamma = 2/6$, i.e., those of Fig. 1(f) and (h), the set of cuts could just as consistently have been chosen in the orthogonal sense to that depicted, without changing the symmetry characteristics at all. Another interesting example is the modified cube. In the modified configuration shown in Fig. 1a, the 'Yin-Yang' grid is obtained. An alternative would be the 'barrel grid' with two polar domains and an intervening cylindrical domain, which is essentially the same topology as the three-grid configuration of grids used in the present global Grid-point Statistical Interpolation (GSI) by which NCEP performs its operational assimilations (e.g., Wu et al. 2002).

Regardless of the angle deficit, γ, or the global symmetries about a given vertex, the incisions that straddle the vertex will always have a unique transverse axis of *local* mirror symmetry in the map space there. In the cases where the angle deficits are of either types 2/4 or 2/6, the incisions are made to share equally the angle deficits (relative to a half-circle) between the two sides of the cut; in the other cases the cuts separate an odd number (one or three) of panel corners on one side from an even number (two) on the other. We shall assume grid configurations in which the grid lines run parallel (in map space) to the edges of the map panels. When two map panels meet at the cut, the symmetric bisector through the corner is their common edge and lines parallel to it in grid space are therefore members of the family of curves that define one of the two horizontal grid coordinates.

If we consider the horizontal metric geometry in which Cartesian distance in map coordinates defines the effective metric (and an implied space that is therefore Euclidean except at the isolated vertex singularities), then all the grid lines can be thought of as geodesics of this particular geometry. This is an intrinsic property of the metric space and remains true even though the metric may be expressed, in tensorial form, in geographical coordinates, or any other smoothly transformed coordinate set. As is well known from standard differential geometry (e.g., Kreysig 1991, Synge and Schild 1949) a geodesic may be extended through space by integrating the second-order equation:

$$\frac{d^2 X^a}{dt^2} = -\Gamma^a_{\ bc} \frac{dX^b}{dt} \frac{dX^c}{dt}, \tag{6.1}$$

where t is a parameter of the geodesic 'trajectory' and,

$$\Gamma^a_{\ bc} = G^{ad} \Gamma_{d\,bc}, \tag{6.2}$$

with

$$\Gamma_{d\,bc} = \frac{1}{2} \left(\frac{\partial G_{dc}}{\partial X^b} + \frac{\partial G_{db}}{\partial X^c} - \frac{\partial G_{bc}}{\partial X^d} \right), \tag{6.3}$$

and contravariant tensor, G^{ad}, being the matrix inverse of G_{ab}. $\Gamma_{d\,bc}$ and $\Gamma^a_{\ bc}$ are coordinate-dependent non-tensors known as the Christoffel symbols of the first kind, and second kind, respectively.

The minor problem we have to address is that this prescription for the geodesic requires the metric tensor to be differentiated with respect to all three coordinate directions, whereas the metric defined in Section 5 assumes only that the metric tensor exists on the unit sphere. However, taking

$$R^2 = \mathbf{X}\cdot\mathbf{X}, \tag{6.4}$$

we can generalize the metric used in (5.18), without altering its trivial prescription over the unit sphere, so that it exists for *any* finite $\mathbf{X}$:

$$G_{ab} = \frac{\delta_{ab}}{R^2}. \tag{6.5}$$

If we were to transform to spherical polar coordinates such that,

$$X^1 = R\cos\phi\cos\theta, \tag{6.6a}$$
$$X^2 = R\cos\phi\sin\theta, \tag{6.6b}$$
$$X^3 = R\sin\phi, \tag{6.6c}$$

then the Riemannian infinitesimal metric distance, ds, would be found to be:

$$ds^2 = (\cos^2\phi\, d\theta^2 + d\phi^2) + \left(\frac{dR^2}{R^2}\right). \tag{6.7}$$

The angle variables appear only in the first parentheses and the radial variable appears only in the second. This full separability implies that t-parameterized geodesics that are initially tangent to a sphere, $dR/dt = 0$, are confined for all t to the same sphere. Moreover, by the invariance of the metric to rotations, these tangential geodesics are necessarily great circles. We can write the components of the Christoffel symbol implied by this choice of metric:

$$\Gamma^a_{\ bc} = \frac{1}{R^2}\left\{\delta_{bc}X^a - \delta^a_c\delta_{bb'}X^{b'} - \delta^a_b\delta_{cc'}X^{c'}\right\} \tag{6.8}$$

We also need to construct another metric, $\hat{G}_{ab}$, such that the straight lines of the developed map, when transformed to their mapping images on the unit sphere, are geodesics with respect to this metric. We start by formally augmenting the map coordinates to three dimensions:

$$\mathbf{x} \equiv (x^1, x^2, x^3)^\mathsf{T} \equiv (x, y, z)^\mathsf{T}, \tag{6.9}$$

where $z = 0$ corresponds to the unit sphere, for which the transformation to $\mathbf{X}$ is already assumed known, and where now:

$$\mathbf{X}(x, y, z) = \mathbf{X}(x, y, 0)\exp(z) \tag{6.10}$$

so that $z = \ln(R)$. The Jacobian operator, $\mathbf{J} = \partial\mathbf{X}/\partial\mathbf{x}$, now has a full 3×3 matrix representation which we can express in terms of its columns in the style:

$$\mathbf{J} = \left[\frac{\partial\mathbf{X}}{\partial x}, \frac{\partial\mathbf{X}}{\partial y}, \frac{\partial\mathbf{X}}{\partial z}\right] = \left[\frac{\partial\mathbf{X}}{\partial x}, \frac{\partial\mathbf{X}}{\partial y}, \mathbf{X}\right] \tag{6.11}$$

with determinant,

$$\Delta = |\mathbf{J}| = \left(\frac{\partial \mathbf{X}}{\partial x} \times \frac{\partial \mathbf{X}}{\partial y} \right) \cdot \mathbf{X} \tag{6.12}$$

and an inverse,

$$\frac{\partial x}{\partial X} \equiv \mathbf{H} = \mathbf{J}^{-1} = \left[\frac{1}{\Delta} \frac{\partial \mathbf{X}}{\partial y} \times \mathbf{X}, -\frac{1}{\Delta} \frac{\partial \mathbf{X}}{\partial x} \times \mathbf{X}, \frac{1}{R^2} \mathbf{X} \right]^{\mathsf{T}}. \tag{6.13}$$

In $\mathbf{x}$-space, a metric tensor satisfying our requirements is simply:

$$\hat{g}_{ij} = \delta_{ij}, \tag{6.14}$$

which therefore transforms to $\mathbf{X}$-space as the covariant metric:

$$\hat{G}_{ab} = H^i_{\ a} H^j_{\ b} \delta_{ij}, \tag{6.15}$$

or the contravariant metric:

$$\hat{G}^{ab} = J^a_{\ i} J^b_{\ j} \delta^{ij}. \tag{6.16}$$

Since, in x-space, a geodesic of this metric must satisfy $d^2\mathbf{x}/dt^2 = 0$, we can deduce that, in $\mathbf{X}$-space, it obeys:

$$\begin{aligned} \frac{d^2 X^a}{dt^2} &= J^a_{ij} \frac{dx^i}{dt} \frac{dx^j}{dt} \\ &= J^a_{ij} H^i_{\ b} H^j_{\ c} \frac{dX^b}{dt} \frac{dX^c}{dt}, \end{aligned} \tag{6.17}$$

where

$$J^d_{ij} = \frac{\partial^2 X^d}{\partial x^i \, \partial x^j}, \tag{6.18}$$

and hence that the $\mathbf{X}$-space Christoffel symbol of the second kind is:

$$\hat{\Gamma}^a_{\ bc} = -J^a_{ij} H^i_{\ b} H^j_{\ c}. \tag{6.19}$$

We will seek to smooth and stretch the grid on either side of an incision at each vertex by reconstructing the mapping of a special family of 'straight' map lines, within a small radius of each vertex, as 'trajectories' that obey a modification of the geodesic equation that involves blending the two Christoffel symbols, Γ and $\hat{\Gamma}$. In order to do this smoothly and consistently, we need to introduce a blending 'weight' function.

For $0 \le \lambda \le 1$, let r_λ define the radius of a disc in map space, such that the diameter, $2r_\lambda$ is λ times the smallest distance between any pair of map singularities. (The largest non-overlapping discs centered at each vertex correspond to $\lambda = 1$.) Define a smooth weighting function, $w(r/r_\lambda)$, of the map-distance, r, to the nearest vertex with the properties:

(i) $w(\rho) = 0$ when $\rho = 0$ and $w(\rho) = 1$ when $\rho \ge 1$;

(ii) $w(\rho)$ is analytic in the open interval, $\rho \in (0, 1)$;

(iii) At least the first few derivatives vanish at $\rho = 0$ and at $\rho = 1$.

While the various polynomial 'incomplete Beta functions' qualify as candidates, this option would involve an arbitrary choice from this family of distributions and, at some degree, the derivatives then cease to remain continuous. If instead we define,

$$w(\rho) = \frac{1}{K}\int_0^\rho \exp\left(-\frac{1}{\rho'(1-\rho')}\right) d\rho' \tag{6.20}$$

where K is the normalizing constant, then we shall have fulfilled the above condition (iii) for *all* degrees of derivatives. The normalizing constant is easily computed by numerical quadrature, but formally evaluates to the Whittaker function (Wang and Guo, 1989):

$$\begin{aligned} K &= \frac{1}{2}e^{-2}\sqrt{\pi}W_{-\frac{1}{2},-\frac{1}{2}}(4) \\ &\approx 0.00702985840660965239241 27, \end{aligned} \tag{6.21}$$

where the latter is defined

$$W_{-1/2,-1/2}(4) = \frac{1}{\sqrt{\pi}}\int_{1/2}^\infty \frac{1}{e^{4t}(t-1/2)^{1/2}(t+1/2)^{3/2}}dt. \tag{6.22}$$

Now consider the behavior of trajectories on the unit sphere near a vertex map point that we shall make the origin, $\mathbf{0}$, of our $\mathbf{x}$-coordinates. We suppose that the trajectories obey the modified geodesic equation,

$$\frac{d^2X^a}{dt^2} = -\tilde{\Gamma}^a_{bc}\frac{dX^b}{dt}\frac{dX^c}{dt}, \tag{6.23}$$

where,

$$\tilde{\Gamma}^a_{bc} = \Gamma^a_{bc} + w(r/r_\lambda)\left(\hat{\Gamma}^a_{bc} - \Gamma^a_{bc}\right). \tag{6.24}$$

Tangency to the unit sphere is preserved by this modification. Outside the 'intervention disc' the trajectories are the $\mathbf{X}$-space images of the straight lines of the map. But inside the disc, the curvature of the trajectories is diluted, especially very close to the center where, in the limit, $|\mathbf{x}| \to 0$, the trajectories 'straighten out' effectively to segments of great circles. For finite λ the curvature of such trajectories remains bounded.

Apart from the exceptional polyhedron of Fig. $1(\ell)$ the existence of a symmetry plane through each polyhedron vertex defines a bilateral symmetry axis of the map through $\mathbf{0}$ and this is either aligned with the map-space coordinate grid or is a diagonal of the grid. For the polyhedral configurations with angular deficit $\gamma = 1/4$ or $\gamma = 1/6$, the axis is parallel to the grid on one side of the singularity, and diagonally oblique to it on the opposite side. In either case, we shall refer to the two families of straight lines of the map parallel to each branch of the symmetry axis, as 'meridians'. The modification of the trajectories allows us to redefine the meridians by integrating them via (6.23) inward and partially through the disc of intervention from both directions. The two families of meridians remain unperturbed from their respective original course outside the intervention disc, but each family now passes smoothly over the original singularity, $\mathbf{0}$, without member meridians crossing one another until they have passed a safe distance *beyond* the singularity (whereupon they intersect in a configuration of caustics).

The map panel corners that meet one side of the nominal dividing incision can collective have a total angle (in map space) at the vertex of either 180°, 120°, 90° or just 60°. The case

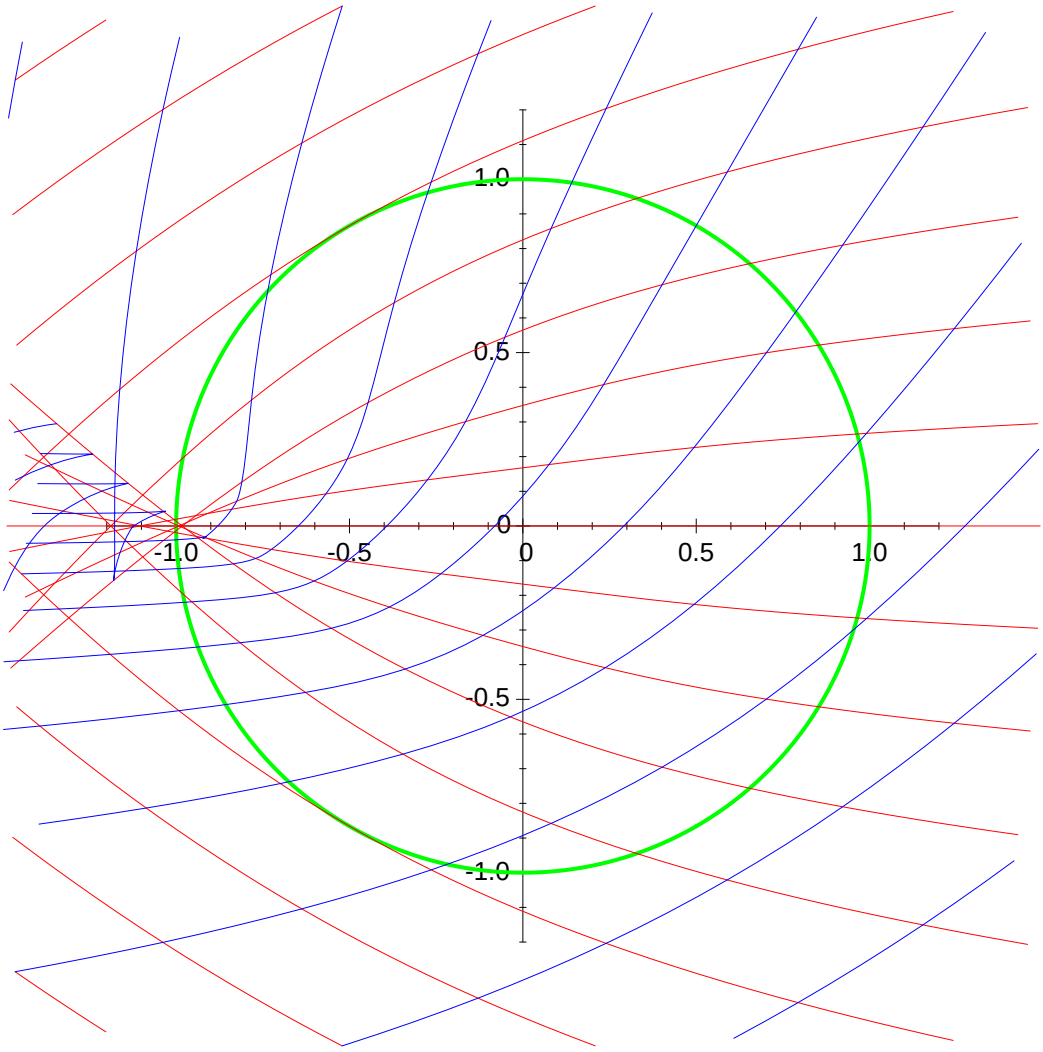

Figure 7. An example of meridians (in red) integrated from the right towards the left through the disc of intervention, and 45° rhumb lines (in blue) intersecting these meridians. Although singularities eventually occur as the meridians are integrated, they occur in caustics far enough beyond the original singularity to be considered outside the eventual finite difference grid.

('case-1') where this angle is 180° is special since it is the only case in which the incoming edge segments (two square corners or three triangle corners) of this piece should merge smoothly as one continuous curve. The other examples, which we refer to collectively as 'case 2', have these edge segments coming together at the vertex and crossing each other transversally when this piece of the map is extrapolated. We treat case 1 first as follows.

(*a*) *Case 1*

The new meridians redefine the coordinate grid lines labeled by, say, '*y*'. The transverse family of grid lines, i.e., those of constant '*x*', that become (in map space) parallel to the overset incision, are constructed by a different procedure, since it is necessary not only that they be

smooth near **0**, but that they properly match up with the old grid lines on both sides of the symmetry axis outside the intervention disc. In this case we use the following modification of the idea of 'rhumb lines'.

A rhumb line, or 'loxodrome' is a curve passing though a family of nonintersecting meridians at a constant angle of intersection. Let us suppose that the coordinate grid we are modifying is that of a conformal mapping where the original Cartesian grid lines in **x**-space formed an orthogonal curvilinear gridding in **X**-space. We would obviously want to preserve this orthogonality for a rectangular gridding of the map, even in the intervention disc, so the use of rhumb lines with orthogonal intersections would accomplish this. The construction of a rhumb line by integration would seem to be an asymmetrical process (we have to start from one side or another) but the existence of bilateral symmetry guarantees that the lines transverse to the meridians continue to respect this symmetry and join up properly outside the intervention disc.

Now suppose that the mapping we are generalizing with oversets is one that is *not* conformal, but rather one of the type, with nonvanishing τ, described in Section 5. In this case, the transverse intersections in the unmodified **x**-coordinate grid involve variable angles of intersection in **X**-space and are not strictly describable as rhumb lines. In this case, for each modified x-labeled rhumb line, we construct a quantity we call the 'obliquity', q, defined as the cosine of the angle of intersection. In the unmodified gridding, this obliquity is recorded, for each (x, y) in the vicinity of the singularity as

$$q(\mathbf{x}) = \frac{\frac{\partial \mathbf{X}}{\partial x} . \frac{\partial \mathbf{X}}{\partial y}}{\left|\frac{\partial \mathbf{X}}{\partial x}\right| \left|\frac{\partial \mathbf{X}}{\partial y}\right|}. \tag{6.25}$$

Except in the conformal case (where it vanishes) $q(\mathbf{x})$ is not a smooth function of $\mathbf{x}$ at the singularity. But if we construct,

$$\hat{q}(\mathbf{x}) = w(|\mathbf{x}|/r_\lambda) q(\mathbf{x}), \tag{6.26}$$

then $\hat{q}(\mathbf{x})$ is certainly smooth, and continues to respect the mapping symmetries. Since, in the case we are presently treating, the family of meridians are destined to become the isolines of the new coordinates, $\hat{y}$, but their 'time-like' parameter, t, is not generally the corresponding final $\hat{x}$ coordinate, we shall conveniently refer to locations on this family of meridians using the temporary mapping coordinates, $\tilde{\mathbf{x}} \equiv (\tilde{x}, \tilde{y})$, where $\tilde{y} = \hat{y}$ corresponds to the original coordinate, y, *before* the trajectory is modified in (and beyond) the intervention disc, $\tilde{x}$ corresponds to the original coordinate x, *before* the onset of intervention and where the synonym, $\tilde{x} = t$, makes for notational consistency. The new family of coordinate lines transverse to the meridians of constant $\hat{y}$ will each be labeled by their unique $\hat{x}$ matching the original x outside the region of influence of the intervention disc, and they will be generated as pseudo-rhumb lines that, at each location $(\hat{x}, \hat{y})$ of the new coordinate-pair, have a cosine of intersection with the meridians given by $\hat{q}(x, y)$. The construction of such pseudo-rhumb lines is as follows.

Let $\mathbf{X}(\tilde{\mathbf{x}})$ denote the location of the meridian labeled $\tilde{y}$ where t along the trajectory attained the value $\tilde{x}$. It is easy to show that the *direction* of the pseudo-rhumb lines must be given by

$$\mathbf{V} = \frac{\partial \mathbf{X}}{\partial \tilde{x}} \hat{q} + \mathbf{X} \times \frac{\partial \mathbf{X}}{\partial \tilde{x}} (1 - \hat{q}^2)^{1/2}. \tag{6.27}$$

Therefore, we integrate the pseudo-rhumb trajectory according to:

$$\frac{\partial \mathbf{X}(\hat{\mathbf{x}})}{\partial \hat{y}} = \mathbf{V}p, \tag{6.28}$$

and seek the p such that, fixing $\hat{x}$,

$$\frac{d\tilde{y}}{d\hat{y}} = 1. \tag{6.29}$$

The value of p that satisfies this condition can be shown to be

$$p = \frac{\mathbf{X} \times \frac{\partial \mathbf{X}}{\partial \tilde{x}} \cdot \frac{\partial \mathbf{X}}{\partial \tilde{y}}}{\mathbf{X} \times \frac{\partial \mathbf{X}}{\partial \tilde{x}} \cdot \mathbf{V}}. \tag{6.30}$$

Finally, the symmetry of the geometrical configuration about the axis, $\hat{y} = \tilde{y} = y = 0$ is preserved, which guarantees that the pseudo-rhumb lines traversing the meridians deviated by the disc of intervention emerge smoothly coincident with the original mapping's corresponding lines of constant x.

(b) *Case 2*

In this case, the meridians are defined exactly as before, except they are not themselves destined to become straight lines of the final map. Instead they are employed merely to provide the orientation of *two* families of pseudo-rhumb lines – one family being parallel to the edge of this piece of the map on one side of the vertex and the other family the mirror image of the first. Also, since the 'ideal' angle of map intersection with the meridians is, in this case, no longer a right angle, we must generalize the formula for the prescribed obliquity of these intersections:

$$\hat{q}(\mathbf{x}) = q_0 + w(|\mathbf{x}|/r_\lambda)(q(\mathbf{x}) - q_0), \tag{6.31}$$

where the 'ideal obliquity' of the map is $q_0 = \pm 1/2, \quad \pm\sqrt{2}/2, \quad \pm\sqrt{3}/2$, as this incision-bounded map piece subtends, 120°, 90°, or 60°, respectively, at the vertex, the sign being determined by the side of the symmetry axis from which the incoming pseudo-rhumb lines are coming. In this case, the symmetric pair of families of pseudo-rhumb lines do include the newly modified grid lines associated with this side of the overset. For the square-griddable polyhedra, this construction continues to ensure that the modification of the conformal version of each grid preserves the orthogonality of the intersections of these new coordinate lines, although the aspect ratios of the grid cells are not generally unity – the overset grids are rectangular-orthogonal but not square-orthogonal, in other words.

(c) *Special oversets modifying conformal grids*

In Section 5 we discussed the universal characteristic scaling of the various vertex singularities at their different stages of migration labeled by τ, where the scaling pertained to the immediate neighborhood of each vertex. But we can imagine that, for each such grid, there is another 'ideal' plane mapping in which the scaling about the image of the vertex becomes

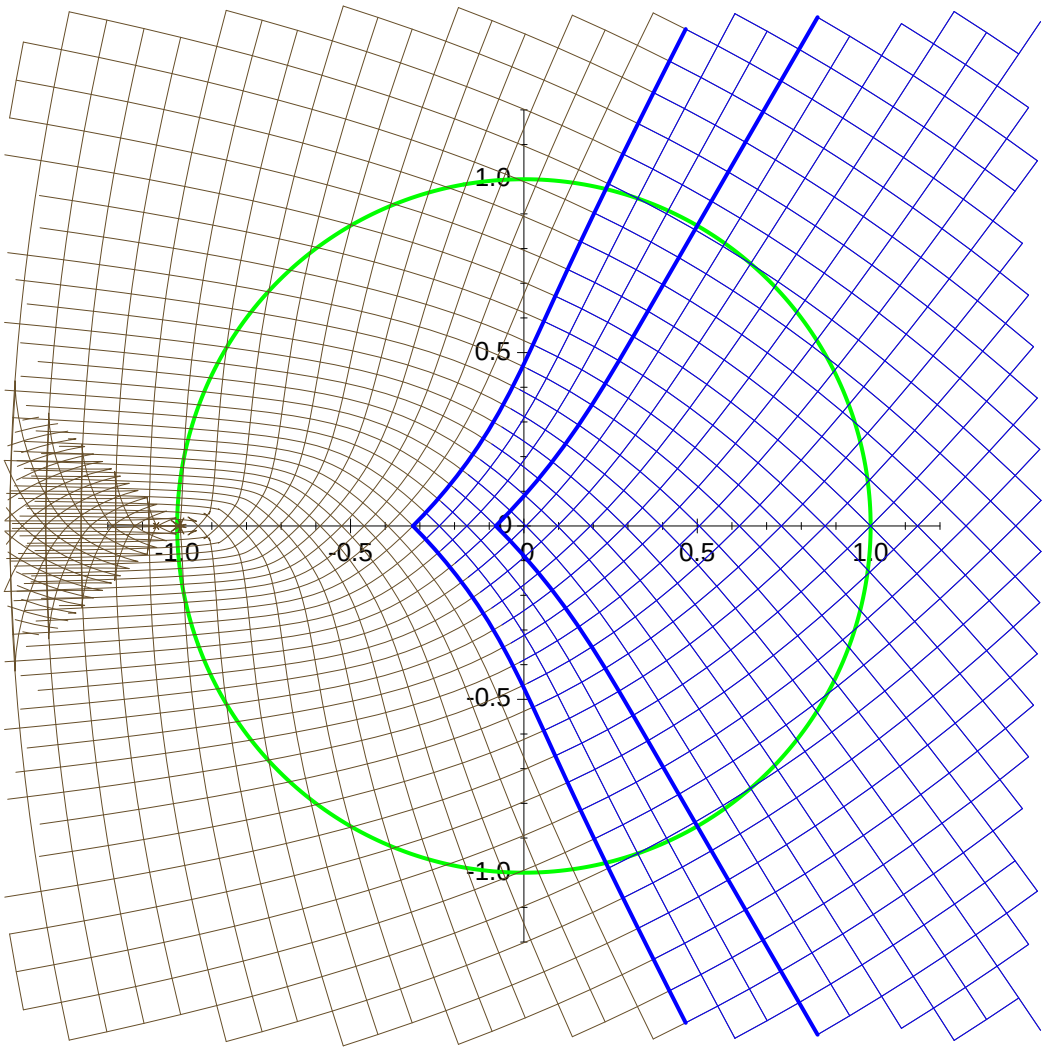

Figure 8. A corner of the reconstructed, formerly conformal, grid showing the symmetrical pair of 45° rhumb lines whose guiding 'meridians' have now been removed. The grid that remains is clearly still orthogonal but the grid cells are manifestly not 'square' in their proportions within the disc of intervention. The original panel boundary (which formerly met the singularity) is modified to the inner heavy blue angled line; the outer heavy blue angled line depicts a possible boundary of the extended grid with the additional margin.

perfect out to any finite radius. In this mapping the distortion of the grid map becomes rotationally symmetric and the radius, R in this ideal plane scales with map-radius r like (5.29), except without any error of approximation at finite r:

$$R = Kr^p. \tag{6.32}$$

If α is the azimuth (about the vertex) in map space, so that Cartesian map coordinates here are given by $(x, y) = (r\cos\alpha, r\sin\alpha)$, and if β is the azimuth in the ideal plane, so that Cartesian coordinates there are given by, $(X, Y) \equiv (X^1, X^2) = (R\cos\beta, R\sin\beta)$, then we also have the

correspondence, independent of the migration stage τ:

$$\beta = q\alpha. \tag{6.33}$$

Just from these *exact* scaling rules, it is possible now to construct the effective metric tensors, the Christoffel symbols analytically (with a constant scale factor) and thus, to perfectly reconstruct the images of all the grid lines in the ideal plane as geodesic trajectories. The singular behavior of the grid in the vicinity of the vertex is now seen to be a direct consequence of the unboundedly large components of Γ^i_{jk} there. Note also that, implicitly, we have defined a unique mapping between the ideal plane and the finite neighborhood of the vertex's image on the sphere, since the mapping to the sphere for the chosen grid topology and τ values was established to be essentially unique by the migration procedure described in the previous section.

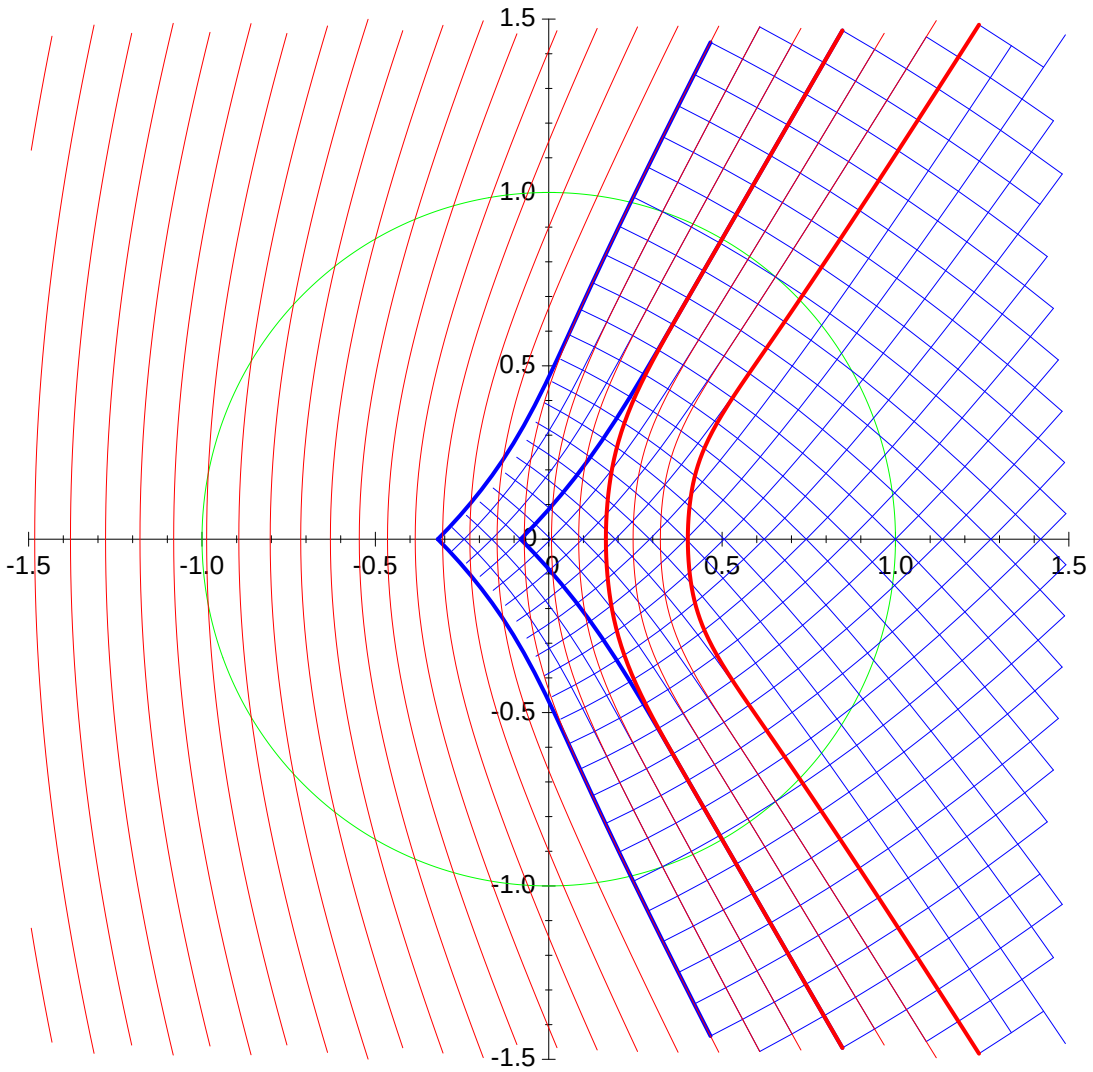

Figure 9. The overset configuration showing both pieces of the modified conformal cubic grid now overlapping within the disc of intervention.

Thus one is tempted to forgo the three-dimensional constructions of meridians and pseudo-rhumb lines in favor of the alternative corresponding construction in this ideal planar representation of the vertex neighborhood. In the case of the conformal mappings there should be no problem with this approach but it unfortunately fails to guarantee a strictly smooth reconstruction of the mapping in the case of the migrated-grid solution (positive *tau*) in the overset regions because the anisotropic components of the map-migration field of Section 5 produce a singularity which does not *purely* comprise the power-law scaling of this idealization (although it is certainly the dominant component). However, these is no objection to using this approach in the case of the conformal maps. In that case, the idealized solution for the conformal map is conveniently obtained by letting r in (6.32) be a complex number representation of the map point, R the corresponding complex number represention of the point on the earth to which it maps, where the coordinate origin of both spaces is the vertex. Since $\hat{g}_{ij}$ remains the trivial metric in r-space, the parameterized geodesics obey $d^2r/dt^2 = 0$, which translates to,

$$\frac{d^2R}{dt^2} = \gamma \frac{1}{R} \frac{dR}{dt} \frac{dR}{dt}, \tag{6.34}$$

for the angular deficit parameter, γ, and hence, the role of the Christoffel symbol, $\hat{\Gamma}$, is here played by the complex function,

$$\hat{\Gamma} = -\frac{\gamma}{R}. \tag{6.35}$$

In place of the 'great circle' geodesics of the metric G_{ab} we have, in this idealization, straight lines in R-space, and so we can take the effective Christoffel symbol, Γ, of this metric to vanish.

Having constructed the geometry of the overset portions of the grid in this idealized complex-number framework, it is straightforward to embed it back into the spherical domain with the scaling of the disc of intervention chosen by λ as before. But now we are not dependent upon the existence of an axis of bilateral symmetry passing through the original mapping singularity, so this construction can be applied to modify with oversets the conformal version of the Yin-Yang mapping associated the polyhedron of Fig 1. We are also able to use the complex variable method to align the axis of an overset of any one of the other polyhedral mappings so that this axis does *not* coincide with a symmetry plane of the polyhedron itself.

An interesting and potentially valuable application of this new freedom is to the construction of an overset modification of the conformal isocahedron gridded, not with the obvious triangular subdivision of the faces, but with an oblique and approximately square grid whose Δx and Δy grid increments are taken to form one of the ratios suggested by the Pell sequences described in Section 4. Figure 10 shows the developed map of such a grid geometry, with the oblique alignment chosen to keep the equator close to one of the continuous grid lines, and with the Pell ratio $4:7$ chosen to approximate $1:\sqrt{3}$. The oversets in this case appear in four copies of a pattern that radiate from a coincident trio of map grid points in the interior (but not at the center) of one of the icosahedron's triangular faces, extending directly in the three directions to the three nearest surrounding vertices, and then slightly beyond in the usual way. Within the intervention discs, the oversets are constructed by the complex variable method, but now suitably rotated about each vertex to align with the rectangular grid, rather than any axis of polyhedral symmetry. Also, in this special case, the reconstruction of the grid lines as pairs of crossing rhumb lines (on the 'case 2' side of the overset cut) the two families of rhumb

line are no longer symmetrical – they cut the meridians at two different angles. Nevertheless, these angles are such that the rhumb lines of one family continue to cut those of the other at right angles, thereby preserving the orthogonality of the rectanguler grid. Immediately around the triple junction of the nominal oversets, the three involved grid pieces are perfectly smooth conformal mappings that, in map space, are just 120° rotations of each other. The only additional complication, and it is only a minor one, is that this configuration implies is that

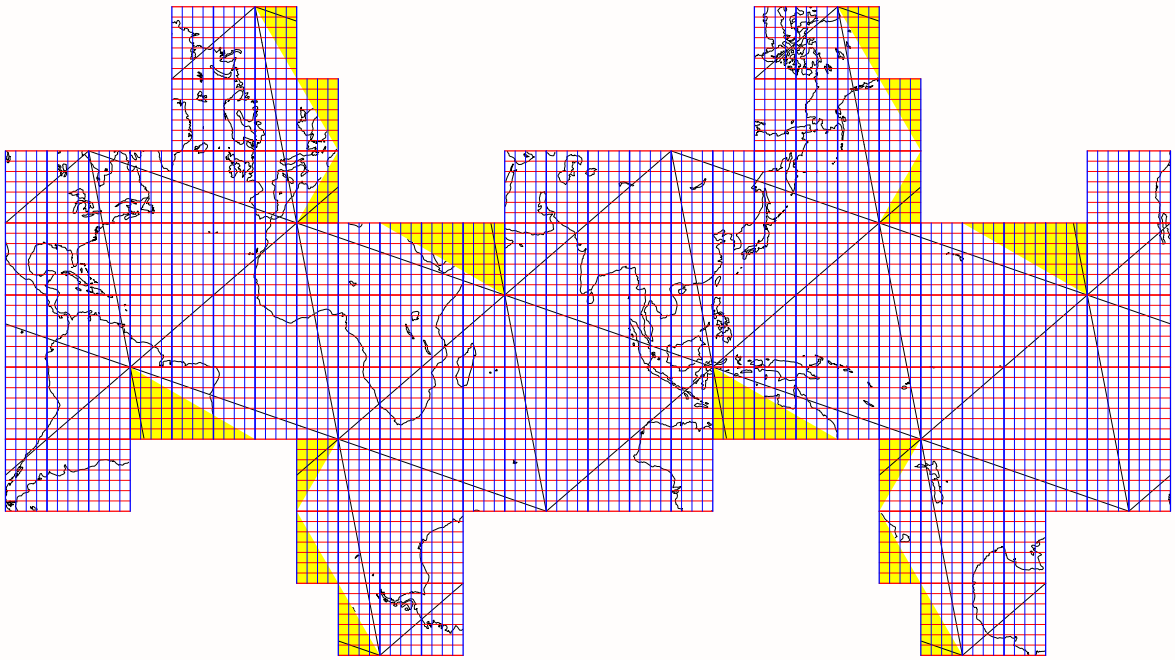

Figure 10. An example of the use of the solutions of the Pell equation, $C^2 - 3S^2 = 1$ to construct a quasi-square rectangular gridding of the regular icoshedron mapped to the surface of the Earth. The mapping combines the advantage of minimal distortion (owing to the adoption of the icosahedral geometry) and numerical convenience associated with the rectangular lattice. The Pell solution allows the two Cartesian resolutions to be approximately equal (for the $C = 7$, $S = 4$ Pell solution shown here, the disparity is only about 1%).

7. Discussion and conclusion

We have described a set of twelve polyhedral types that appear to allow useful square or triangular griddings, and we have introduced a set of standardized techniques by which the grids associated with these geometries can be forged into practical computational lattices on the surface of the sphere. The process can be summarized as follows:

(i) The selection of the suitable polyhedron (which may include the specification either of two integer aspect parameters, (a, b) or of an equivalent 'Pell index', in the case where the specific polyhedron belongs to a family of a given type);

(ii) The construction of the conformal spherical mapping respecting the polyhedron's symmetries;

(iii) The optional 'map migration' to smooth out the inequities of the Jacobian of the mapping, applied to the degree prescribed by the nonnegative real parameter $\tau \leq 1$;

(iv) The optional 'oversetting' procedure to remove the mapping singularities associated with the polyhedral vertices, with the fraction of the segment between neighboring vertices lying within the disc of intervention being parameterized by the nonnegative real $\lambda \leq 1$.

We have provided an outline of the telescoping multigrid structure we need in performing the stages (ii) and (iii) above, and which can help with the accurate resolution of mapping details near the singularities when they are removed in stage (iv).

The methods proposed are standard across all sufficiently symmetrical and griddable polyhedra. Because they are defined with mathematical precision by discrete symmetry and aspect indices, and just two continuously-adjustable real parameters (the area-smoothing parameter, τ, and the optional overset size parameter, λ), it is possible to carry out the mappings, 'on demand' using a single generic computational procedure that applies to all of the geometries depicted in Fig. 1(a)–(k), whose vertices each lie on a plane of dihedral symmetry of the polyhedron. Although the options are more restricted in the less symmetrical example exhibited by the polyhedron of Fig. 1(ℓ), even here it is possible to construct the unique symmetry-preserving conformal grid ($\tau = 0$, $\lambda = 0$), or an orthogonal overset grid variant of it ($\lambda > 0$) according to the procedure set out in section 6c.

When the overset option is exercised ($\lambda > 0$) and the vertex singularies are removed from the computational grid, there is a need to carry out interpolations and blending of solutions in the regions of overlaps. Our overset construction differs from others that have been described (Phillips 1957, Starius 1980, Browning et al. 1989, Kageyama and Sato 2004) in that, for a $\lambda < 1$ where the discs of intervention certainly do not touch, there remains between the neighboring vertices edge mid-sections across which the grid remains perfectly smooth and continuous. Obviously, this implies the computational advantage that these is no need for mutual interpolation and blending between grid solutions here, reducing the amount of computation in a model needed at each time step. But it also means that, in a model whose numerics enjoy certain inherent conservation principles by virtue of the construction of the finite difference formulation, the places where this conservation is formally lost through the overset solution reconciliations are relatively small and isolated regions. Then a form of 'constraint restoration', applied only, and separately, within each disc of intervention might be more effective than its more usual, scatter-shot, global application (e.g., Priestley 1993).

The oversetting methods described here are strictly local modifications to the grid, confined within a specified disc surrounding each vertex. In the cases where the map migration stage (partially of fully equalizing the absolute map Jacobians) is omitted, we have shown that it is

possible to ensure that, even in the overset regions where the grid is modified, the modification can be made to preserve perfect orthogonality for rectangular grids. The question that comes to mind is: can another oversetting procedure produce grids that remain, not just orthogonal, but fully conformal? This is formally possible by exploiting the concept of a 'Riemann surface' of complex analytic function theory to produce a suitable overlap at points arrived at by paths from a common origin that pass on opposite sides of one of a pair of 'branch points' approximately straddling the location of the original vertex. For the geometries of sufficient symmetry, the pursuit of the fully conformal solution to the oversetting problem should prove numerically advantageous, as it allows almost any regional grid point model, whether employing a square or a triangular grid, to be globally generalized with virtually no change whatsoever needed in its core numerics. Unlike the solutions described here, such fully conformal oversets involve adjustments to the unadorned conformal mapping grid that can no longer be confined within the bounds of finite-radius vertex-centered discs – a fully conformal solution is necessarily global and can, in principle, be reconstructed (by analytic continuation) in its entirety from even the smallest finite fragment of it. A description of the special generation procedures entailed is beyond the scope of this note but will be comprehensively described in a sequel.

A variant of the same special procedure of section 6c applied in a *non-standard* way to the conformal icosahedron even allows a *rectangular* (but almost square) and perfectly orthogonal smooth overset grid to be constructed within the global icosahedral framework (Fig. 10). The proportions of the rectangular grid involve the Pell theory of section 4 in order to ensure that the grid conforming to the equilateral triangular panels closely approximates a square grid. Although the resulting oversets are more extensive than those of the other geometries we have considered, this example shows that the admirable mapping efficiency and low distortion possessed by the icosahedral geometry can, in principle, also be enjoyed by a model framed within the more conventional orthogonal rectangular grid paradigm.

By standardizing the specification and construction of these global grids we facilitate the fair intercomparison of methods as applied to them. The sequel, Part II (Rančić and Purser, 2012) will exhibit some of these intercomparisons in grid geometries constructed in accordance with the prescriptions we have laid out in this article.

Acknowledgments

This work is largely a development that has grown from a presentation given at the 2010 Workshop on the Solution of Partial Differential Equations on the Sphere, held at the Alfred Wegener Institute, Potsdam, Germany, Aug. 24–27, 2010. We are grateful to the organizers and sponsors of that program, and to the AWI staff for their hospitality. M. Rančić gratefully acknowledges the generous support received from the National Science Foundation through the receipt of grant ATM-0739518. The authors also thank Drs. Sajal K. Kar and David F. Parrish for their helpful reviews.

Appendix A

The vertex-symmetric finite griddings of the sphere

The finite polyhedral gridding of the sphere require at least three vertices (since an angular deficit of 2π implied by a two-vertex map leads to a logarithmic singularity in the conformal map, and therefore an infinite extent of at least one map coordinate). If we stipulate that the vertices of the mapping are to be symmetric with respect to the group of symmetries, the list of the basic types of such mappings and their characterizing symmetry groups is easily tabulated.

We shall split the list into those polyhedral geometries that admit square grids, and those that admit equilateral triangular grids on their surfaces. The group of symmetries is required not only to map the polyhedron into itself, but must also map the inscribed grid into itself. For some polyhedra, such as the cube, the square gridding in which the lines of the grid run parallel to the edges of the cube can be distinguished as a separate type from the gridding where the lines runs at 45° to the edges, although the symmetry group in both cases is the same (the full octahedral group of order 48). The former type will be referred to by its two-character code 'cu' and is most simply exemplified by a configuration with six map panels; the latter will be referred to here by its code, 'ce' and has, as its simplest exemplar, the configuration with 12 map panels. However, there are also many ways to grid the cube's surface where the grid lines form other oblique angles to the edges, and the pattern is then endowed with a chirality that prevents reflections from belonging to the group of symmetries; the group in this case is the *chiral* octahedral group of order 24. The code we use to refer to this class of chiral cubic grid geometries is 'cc' and we note that the simplest member is a configuration with 30 map panels and with the edges pointing along directions such as vector $(2, 1)$ in map coordinates. There are other geometries, such as the class of octagonal dihedra (code 'oc'), where rotating the grid by 45° and shrinking it by a (linear) factor of $\sqrt{2}$ does not lead to a grid geometry of a new type. In Table 5 we list all the square-griddable polyhedral geometries and their two-character type codes, and signify the existence of a distinguishable class of grids at 45° from the smallest (in panel count) configuration by an 'orientability code' (O.C.) checked as an 'X' or 'XX' when the rotated form is indeed a separate and distinguishable type, and where the 'XX' signifies that, amongst the rotated types are configurations that *do not* have the simpler (unrotated) counterpart with half as many panels.

The group is indicated in each case by its Schönflies and orbifold signatures, N_g being the order of the group. The vertex type, V, is just the angular deficit measured here in right angles. $N_{\min}$ is the size (in panels) of the simplest examplar of each geometry, there being two entries (just as there are two abbreviation codes) wherever an 'X' or 'XX' appears in the O.C. column.

The achiral cubes (cu and cc) may be regarded as special, and more symmetric, cases of the square prism types (sp and sr). The prism analogue of the chiral cube (cc) belongs to a class of configurations, the square screw ('ss'), that also include generalizations of the square antiprism ('sa') to the cases where the 'twist' between the opposing square faces is not simply 45°. As we further reduce the symmetry, and therefore generalize, the square prism, we find the griddings associated with a general cuboid, or rectangular-section prism, or 'alternating sides quadrilateral' prism, to use a terminology that has a direct analogue when we consider the triangular griddings. This polyhedral shape has griddings with lines parallel (code 'ap') and 45° oblique (code 'ar') to edges. The antiprisms of rectangular ends, types 'aa' and 'an', now involve a 90° twist between these ends and, with the orientation code of 'XX', provides the first exhibit where the type 'an', whose grid lines are 45° to the edges of the end rectangles, includes members whose polyhedra cannot be gridded in the style of the type 'aa', where grid lines are

TABLE 5. The finite vertex-symmetric square-griddable polyhedra and their symmetries. Each distinct type of grid symmetry is assigned its own unique two-character abbreviation, or 'code'. For some polyhedra, such as the cube, there exist two possible grid orientations, 45° apart, such that both preserve the full symmetry of the polyhedron, and yet both are distinguishable grid types with respect to that symmetry. The orientability code, 'O.C.' is marked 'X' when the two orientations do indeed constitute distinguishable symmetry types; marked 'XX' when the second type comprises some members that are not simply derivable from a member of the first type by a $\times 2$ diagonal subdivision of its grid-panels; left unmarked when the diagonal orientation is already included in the existing classification (as is the case for antiprisms and for all chiral types). The group is defined by the Schöflies and orbifold signatures, its order being N_g. The vertex type, V, denotes the number of right-angles (i.e., units of 90°) of angular deficit of each vertex. N_{MIN} denotes the size, in square map panels, of the smallest exemplar of each type; when of orientability type X or XX, the second number is size of the smallest exemplar of the second orientation.

Code		Polyhedron type	O.C.	Group		N_g	V	N_{min}	
cu	ce	cube	X	O_h	$\star 432$	48	1	6	12
cc		chiral cube		O	432	24	1	30	
sp	sr	square prism	X	D_{4h}	$\star 224$	16	1	10	20
oc		octagonal dihedron		D_{4h}	$\star 224$	16	1	14	
sa		square antiprism		D_{4d}	$2\star 4$	16	1	8	
ss		square screw		D_4	224	8	1	18	
ap	ar	alt-quad prism	X	D_{2h}	$\star 222$	8	1	22	44
aa	an	alt-quad antiprism	XX	D_{2d}	$2\star 2$	8	1	22	26
sh	se	square dihedron	X	D_{4h}	$\star 224$	16	2	2	4
sc		chiral square dihedron		D_4	224	8	2	10	
ep	er	edge prism	X	D_{2h}	$\star 222$	8	2	4	8
ea	en	edge antiprism	XX	D_{2d}	$2\star 2$	8	2	8	6
es		edge screw		D_2	222	4	2	12	

parallel to the edges of the end rectangles. This exhausts the possible types of vertex-symmetric polyhedral gridding with 90° of angular deficit at each of eight vertices. Fig. 11 illustrates the 'nets' or developments of the polyhedra of the simplest exemplars of each of the aforementioned types colored in conformance with the symmetries of each type. The number in brackets beside each type code gives the number of panels in the exemplar shown. The polyhedron vertices are marked by the black partial discs.

There also exist geometries with four vertices at which the angular deficit is 180°. The square dihedron with the two achiral orientations (codes 'sh' and 'se') or chiral orientations (code 'sc') are the simplest examples. A prism whose section is just an edge (codes 'ep' and 'er') generalizes this dihedron to one of rectangular form (thereby lowering the symmetry of these achiral forms). But we can equally consider what we might refer to as the 'edge antiprism' (actually a tetrahedron, codes 'ea' and 'en') where the 'ea' form has grid lines parallel to the end edges. The 45° rotated form, 'en' is a second example with the orientation code 'XX'. Finally, with a general oblique 'twist' between end edges we obtain an even less symmetrical chiral tetrahedron, referred to here as an 'edge screw' (code 'es') with an order-four group. The illustrations of surface developments of these four-vertex polyhedra are shown in Fig. 12.

A similar tabulation of the triangular-griddable vertex-symmetric polyhedra is provided in Table 6.

TABLE 6. The finite vertex-symmetric equilateral triangular-griddable polyhedra and their symmetries. The tabulation is as in Table 5 except the vertex type, V measures the angular deficit in units of 60° and the orientability code signifies the presence (or not) of grids of distinguishable symmetries when the grid is reoriented by an angle of 30°.

Code		Polyhedron type	O.C.	Group		N_g	V	$N_{\min}$	
ih	ie	icosahedron	X	I_h	$\star 532$	120	1	20	60
ic		chiral icosahedron		I	532	60	1	140	
hp	hr	hexagonal prism	XX	D_{6h}	$\star 226$	24	1	36	60
ha	hn	hexagonal antiprism	XX	D_{6d}	$2\star 6$	24	1	24	48
hs		hexagonal screw		D_6	226	12	1	72	
do		dodecagonal dihedron		D_{6h}	$\star 226$	24	1	96	
tt	tr	truncated tetrahedron	X	T_d	$\star 332$	24	1	28	84
tb		bevelled tetrahedron		T_d	$\star 332$	24	1	40	
oi		octa-icosahedron		T_h	$3\star 2$	24	1	92	
ti		tetra-icosahedron		T	332	12	1	44	
ap	ar	alt-hex prism	XX	D_{3h}	$\star 223$	12	1	62	114
aa	an	alt-hex antiprism	XX	D_{3d}	$2\star 3$	12	1	44	132
oh	oe	octahedron	X	O_h	$\star 432$	48	2	8	24
oc		chiral octahedron		O	432	24	2	56	
hh	he	hexagonal dihedron	X	D_{6h}	$\star 226$	24	2	12	36
hc		chiral hexagonal dihedron		D_6	226	12	2	84	
dp	dr	triangular prism	XX	D_{3h}	$\star 223$	12	2	14	18
da	dn	triangular antiprism	XX	D_{3d}	$2\star 3$	12	2	20	36
ds		triangular screw		D_3	223	6	2	20	
ah	ae	alt-hex dihedron	X	D_{3h}	$\star 223$	12	2	26	78
th	te	tetrahedron	X	T_h	$\star 332$	24	3	4	12
tc		chiral tetrahedron		T	332	12	3	28	
ep		edge prism		D_{2h}	$\star 222$	8	3	8	
ea	en	edge antiprism	XX	D_{2d}	$2\star 2$	8	3	12	20
es		edge screw		D_2	222	4	3	24	
dh	de	triangular dihedron	X	D_{3h}	$\star 223$	12	4	2	6
dc		chiral triangular dihedron		D_3	223	6	4	14	

The achiral rotated grid types, such as for the icosahedron (types 'ih' and 'ie') now involve a relative rotation of 30°, and such a rotation allows one gridding to be replaced by another when the linear size of the grid spacing is reduced by a linear factor of $\sqrt{3}$. Thus the simplest icosahedron of the rotated type, 'ie', has 60 map panels compared to the basic icosahedron of type 'ih' which has 20. There are also chiral versions of the icosahedron (code 'ic') and the obliquity needed to produce the simplest type of this and several other chiral polyhedral geometries involves a seven-fold increase in the number of map panels over the basic form – 140 panels in this case, as the development net illustrates in Fig. 13. There are many analogues to the square-griddable polyhedra where we replace 'square' by (regular) 'hexagon'. The twist between the ends of the hexagonal antiprism (codes 'ha' and 'hn') amounts to the expected

30°, and the more general (and less symmetric) hexagonal screw ('hs') involves either another amount of end-twist or an orientation of the grid whose obliquity with respect to the end-edges is *not* some multilple of 30°. The dodecagonal dihedron (code 'do') is obviously analogous to the square-griddable octagonal dihedron. But there are a few additional geometries that have no square-griddable analogues. The achiral polyhedron comprising four triangles and four hexagons (that are not necessarily regular, but must then be of the 'alternating sides' type), obtained by truncating the corners of a regular tetrahedron is griddable with grid lines parallel to edges of the triangles (type 'tt') or at 30° to these edges (type 'tr'). The symmetry group is that of the full achiral tetrahedron. If the edges of the tetrahedron are bevelled, another polyhedron (code 'tb') admitting a triangular gridding is formed, but now with two sets of four triangles mediated by six rectangles. The grid lines are either parallel to the edges of one set or the other of these triangular faces so the single type suffices. The 'octa-icosahedron' ('oi') is an achiral irregular icosahedron also with two sets of four equilateral triangular faces, but now these are mediated by 12 isosceles triangles in a configuration whose symmetry is that of the pyritohedral group, so that the two sets of equilateral triangles become mirror-images of each other. (The regular icosahedron can be regarded as a special case of this geometry where the isosceles triangles are also equilateral.) A chiral generalized icosahedron with (chiral) tetrahedral symmetry is what we call the 'tetra-icosahedron' (code 'ti'). Two sets of four equilateral triangles are now mediated by 12 congruent scalene triangles. The alternating-sides hexagon (abbreviated 'alt-hex' in the table) is an end shape associated with both prisms (types 'ap' and 'ar') and antiprisms (types 'aa' and 'an'). The simplest exemplars of all these 60°-deficit polyhedra are illustrated in Fig. 13.

With 120° deficits, we have 13 other triangular-griddable types. The regular octahedron exsists in its two achiral types, 'oh' and 'oe', as well as its chiral type, 'oc'. Likewise, the (regular) hexagonal dihedron has its two achiral types 'hh' and 'he', as well as its less symmetrical chiral type, 'hc'. Both the triangular prisms and antiprisms have the orientability codes 'XX' signifying that the forms ('dr' and 'dn') where the grid is oblique to the edges of the end triangles include members where the polyhedron is not griddable by a simpler form (type 'dp' or 'da') with grid lines parallel to the end-edges. Polyhedra whose opposing equilateral 'ends' are mediated by two distinctly different-shaped families of three triangles are reffered to as 'triangular screws' (code 'ds') and form a chiral type whose group is only of order six. Finally for these 120°-deficit shapes, there is an achiral dihedron type of the 'alt-hex' shape (codes 'ah' and 'ae') with the two possible grid orientations. These polyhedra are exemplified in Fig. 14.

Seven distinct gridding types exist with four vertices (angular deficit of 180°), beginning with the two orientations of the achiral tetrahedral types ('th' and 'te') and the chiral form ('tc'). The edge prism ('ep') exists, but now in only one type of orientation, but the edge antiprism (irregular, but achiral tetrahedron) exists in two achiral grid orientations ('ea' and 'en'). The chiral generalization, the 'edge screw' of type 'es' has, as in the square-griddable case, the lowest symmetry (order four). These are illustrated in Fig. 15.

To complete the set of possible griddable polyhedra, we must include the triangular dihedron in its two achiral grid orientations (codes 'dh' and 'de') and its chiral form, 'dc'. The simplest exemplars of these polyhedral griddings are illustrated in the form of their development nets in Fig. 16. The angular deficit of 240° at each vertex makes a geometry of this type rather unattractive for any kind of numerical work on the sphere, of course.

References

Baumgardner, J. R., and P. O. Frederickson	1985	Icosahedral discretization of the two-sphere. *SIAM J. Numer. Anal.*, **22,** 1107– 1115.
Browning, G. L., J. J. Hack, and P. N. Swarztrauber	1989	A comparison of three numerical methods for solving differential equations on the sphere. *Mon. Wea. Rev.,* **117,** 1058–1075.
Chesshire, G., and W. Henshaw	1990	Composite overlapping meshes for the solution of partial differential equations. *J. Comput. Phys.,* **90,** 1–64.
Conway, J. H., O. Delgado Friedrichs, D. H. Huson, and W. P. Thurston	2001	Three dimensional orbifolds and space groups. *Contrib. Algebra. and Geom.,* **42,** 475–507.
Conway, J. H., and D. A. Smith	2003	*On Quaternions and Octonions; Their Geometry.* A. K. Peters, 176 pp.
Conway, J. H., H. Burgiel, and C. Goodman-Strauss	2008	*The Symmetry of Things.* A. K. Peters, 426 pp.
Courtier, P., and J.-F. Geleyn	1988	A global numerical weather prediction model with variable resolution: Application to the shallow-water equations. *Quart. J. Roy. Meteor. Soc.*, **114,** 1321–1346.
Coxeter, H. S. M.	1973	*Regular polytopes*, Dover, New York. 321 pp.
Cullen, M. J. P.	1974	Integrations of the primitive equations on a sphere using the finite-element method. *Quart. J. Roy. Meteor. Soc.*, **100,** 555–562.
Gates, W. L., and C. A. Riegel	1962	A study of numerical errors in the integration of barotropic flows on a spherical grid. *J. Geophys. Res.*, **67,** 773–784.
Giraldo, F. X.	1997	Lagrange-Galerkin methods on spherical geodesic grids. *J. Comput. Phys.*, **136,** 197–213.
Heikes, R., and D. A. Randall	1995a	Numerical integration of the shallow-water equations on a twisted icosahedral grid. Part I: Basic design and results of tests. *Mon. Wea. Rev.,* **123,** 1862-1880.
Heikes, R., and D. A. Randall	1995b	Numerical integration of the shallow-water equations on a twisted icosahedral grid. Part II: A detailed description of the grid and an analysis of numerical accuracy. *Mon. Wea. Rev.*, **123,** 1881–1887.
Henshaw, W.	1994	A fourth-order accurate method for the incompressible Navier- Stokes equations on overlapping grids. . *Comput. Phys.,* **113,** 13–25.
Kageyama, A., and T. Sato	2004	The "Yin-Yang grid": An overset grid in spherical coordinates. *Geochem., Geophys. Geosyst.,* **5,** Q09005, *doi: 10.1029/2004GC000734.arXiv.org:physics/0403123*
Kreyszig, E.	1991	*Differential Geometry* Dover, New York. 352 pp.
Kurihara, Y.	1965	Numerical integration of the primitive equations on a spherical grid. *Mon. Wea. Rev.*, **93,** 399–415.
Lee, L. P.	1976	*Conformal Projections based on Elliptic Functions.* Supplement No. 1 to *Canadian Cartographer,* **Vol. 13,** 128 pp.
Lee, L., R. Bleck, A. E. MacDonald, J. W. Bao, S. Benjamin, J. Middlecoff, N. Wang, and J. Brown	2007	FIM: A vertically flow-following finite-volume icosahedral model. Preprints, 22nd Conference on Wea. Analysis and Forecasting/18th Conference on Num. Wea. Pred., 24–29 June 2007, Park City, UT, Amer. Meteor. Soc.

Majewski, D.	1998	The new global icosahedral-hexagonal gridpoint model GME of the Deutcher Wetterdienst. ECMWF Seminar Proceedings, "Recent developments in numerical methods for atmospheric modelling", 7–11 Sep. 1998. (Available from ECMWF, Reading UK, pp. 172–201.
Masuda, Y., and H. Ohnishi	1986	An integration scheme of the primitive equations model with an icosahedral-hexagonal grid system and its application to the shallow water equations. Proc. WMO/IUGG Symposium on Short- and Medium-Range Numerical Weather Prediction. Tokyo, Japan, Japanese Meteorological Society, 317–326.
McGregor, J. L.	1996	Semi-Lagrangian advection on conformal-cubic grids. *Mon. Wea. Rev.,* **124,** 1311–1322.
Phillips, N. A.	1957	A map projection system suitable for large-scale numerical weather prediction. *J. Meteor. Soc. Japan, 75th Anniversary Volume.* 262–267.
Priestley, A.	1993	A quasi-conservative version of the semi-Lagrangian advection scheme. *Mon. Wea. Rev.,* **121,** 621–629.
Purser, R. J.	1998	Non-standard grids. ECMWF Seminar Proceedings, "Recent developments in numerical methods for atmospheric modelling", 7–11 Sep. 1998. (Available from ECMWF, Reading UK), pp. 44–72.
Purser, R. J.	2004	The bi-Mercator grid as a global framework for numerical weather prediction. (Abstract), The 2004 Workshop on the solution of partial differential equations on the sphere. Yokohama, Japan. Available at *http://www.jamstec.go.jp/frsgc/eng/workshop/pde2004/*
Purser, R. J., and Rančić, M.	1997	Conformal octagon: an attractive framework for global models offering quasi-uniform regional enhancement of resolution. *Meteor. Atmos. Phys.,* **62,** 33–48.
Purser, R. J., and Rančić, M.	1998	Smooth quasi-homogeneous gridding of the sphere. *Quart. J. Meteor. Soc.,* **124,** 637–647.
Putman, W. M., and S.-J. Lin	2007	Finite-volume transport on various cubed-sphere grids. *J. Comput. Phys.,* **227,** 55–78.
Rančić, M., Purser, R. J. and Mesinger, F.	1996	A global shallow-water model using an expanded spherical cube: Gnomonic versus conformal coordinates. *Quart. J. Roy. Meteor. Soc.,* **122,** 959–982.
Rančić, M., and R. J. Purser	2012	A standardized procedure for the derivation of smooth and partially overset grids on the sphere associated with polyhedra that admit regular griddings of their surfaces. Part II: Comparative assessments of numerical accuracy and computational performance. *NOAA/NCEP Office Note (In preparation).*
Rančić, M., and Zhang, H.	2006	Variable resolution on quasi-uniform grids: linear advection experiments. *Meteorol. Atmos. Phys.,* **93,** 97–114.
Rančić, M., H. Zhang, and V. Savcic-Jovcic	2006	Nonlinear advection schemes on the octagonal grid. *Mon. Wea. Rev.,* **136,** 4668–4686.
Ronchi, C., Iacono, R. and Paolucci, P. S.	1996	The 'cubed sphere': A new method for the solution of partial differential equations in spherical geometry. *J. Comp. Phys.*, **124,** 93–114.
Sadourny, R.	1972	Conservative finite-differencing approximations of the primitive equations on quasi-uniform spherical grids. *Mon. Wea. Rev.*, **100,** 136–144.

Sadourny, R., Arakawa, A. and Mintz, Y.	1968	Integration of the nondivergent barotropic vorticity equation with an icosahedral-hexagonal grid for the sphere. *Mon. Wea. Rev.*, **96,** 351–356.
Schmidt, F.	1977	Variable fine mesh in spectral global models. *Contrib. Atmos. Phys.*, **50,** 211–217.
Sharma, B. D.	1982	Crystallographic and Spectroscopic Symmetry Notations. *J. Chem. Educ.,* **59,** 554–557.
Staniforth, A. and J. Thuburn	2012	Horizontal grids for global weather and climate prediction models: a review. *Quart. J. Roy. Meteor. Soc.,* **138,** (to appear.)
Starius, G.	1980	On composite mesh differencing methods for hyperbolic differential equations. *Numer. Math.*, **35,** 241–255.
Synge, J. L., and A. Schild	1949	*Tensor Calculus.* Dover, New York, 324 pp.
Thomas, S. J., and R. D. Loft	2000	Parallel semi-implicit spectral element methods for atmospheric general circulation models. *J. Sci. Comput.*, **15,** 499–518.
Thompson, J. F., Z. U. A. Warsi, and C. W. Mastin	1985	*Numerical Grid Generation: Foundations and Applications*, North-Holland, New York.
Thuburn, J.	1997	A PV-based shallow-water model on a hexagonal-icosahedral grid. *Mon. Wea. Rev.*, **125,** 2328–2347.
Tomita, H., M. Satoh, and K. Goto	2002	An optimization of the icosahedral grid modified by spring dynamics. *J. Comp. Phys.,* **183,** 307–331.
Wang, Z. X., and D. R. Guo	1989	*Special Functions,* World Scientific .
Williamson, D. L.	1968	Integration of the barotropic vorticity equation on a spherical geodesic grid. *Tellus*, **20,** 642–653.
Williamson, D. L.	1970	Integration of the primitive barotropic model over a spherical geodesic grid. *Mon. Wea. Rev.*, **98,** 512–520.
Wu, W.-S., R. J. Purser, and D. F. Parrish	2002	Three-dimensional variational analysis with spatially inhomogeneous covariances. *Mon. Wea. Rev.,* **130,** 2905–2916.
Zhang, H., and M. Rančić	2006	Global Eta model on quasi-uniform grids. *Quart. J. Roy. Meteor. Soc.,* **133,** 517–528.

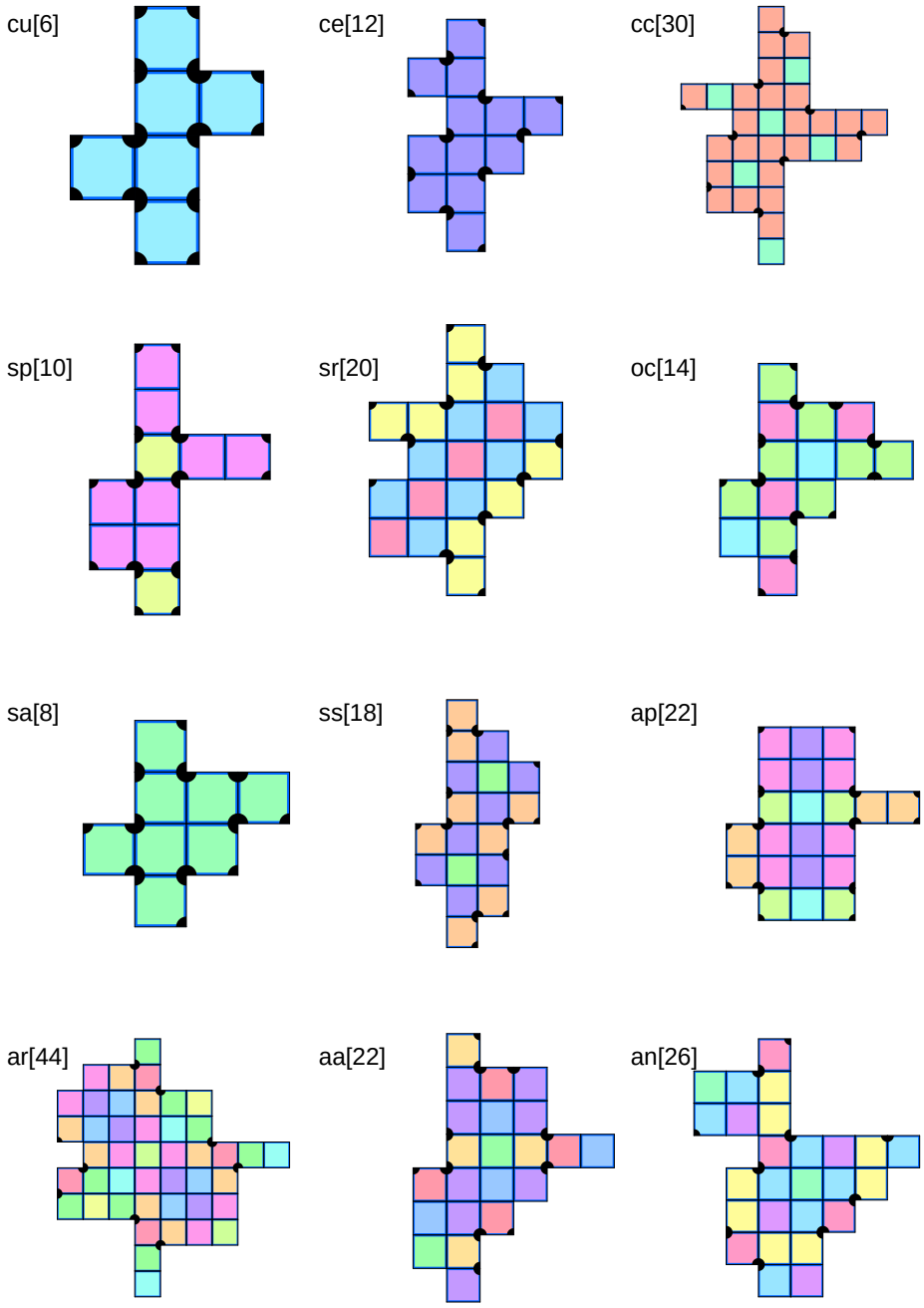

Figure 11. Developments, or 'nets' of the complete surfaces of the polyhedra that correspond to the simplest exemplars of each type of vertex-symmetric square-griddable polyhedron with vertex angular deficit of one right-angle. The labels codes are those used in the classification of Table 5.

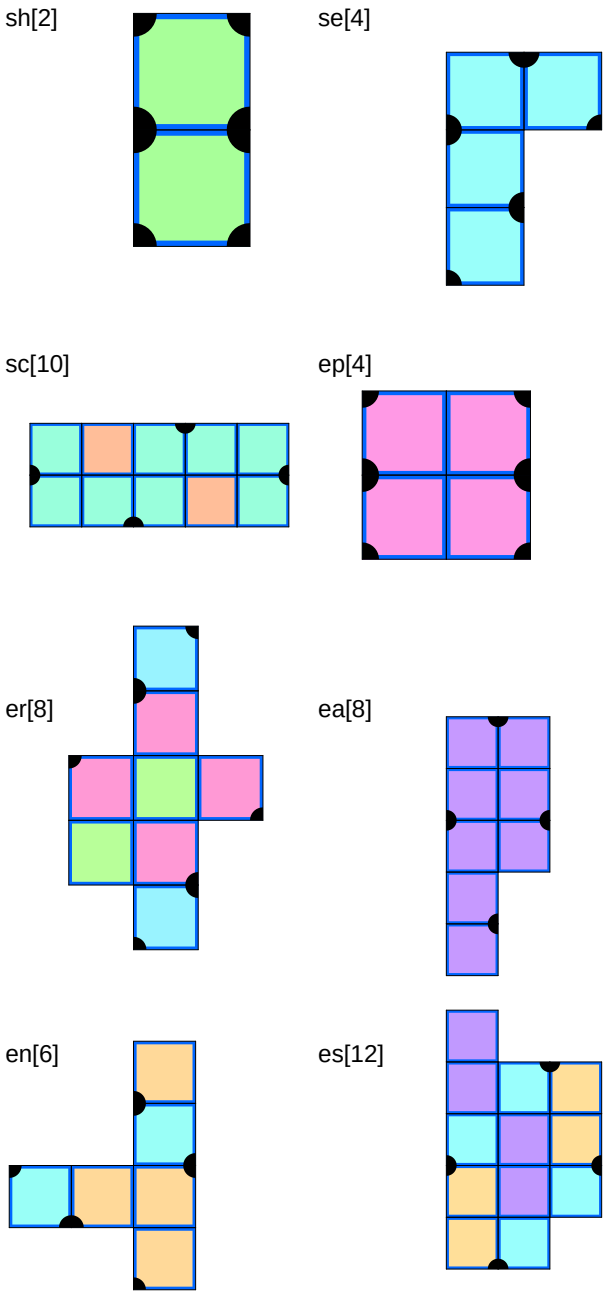

Figure 12. Like Fig. 11 but with the nets corresponding to simplest exemplars of square-griddable polyhedra with vertex angular deficits of two right angles.

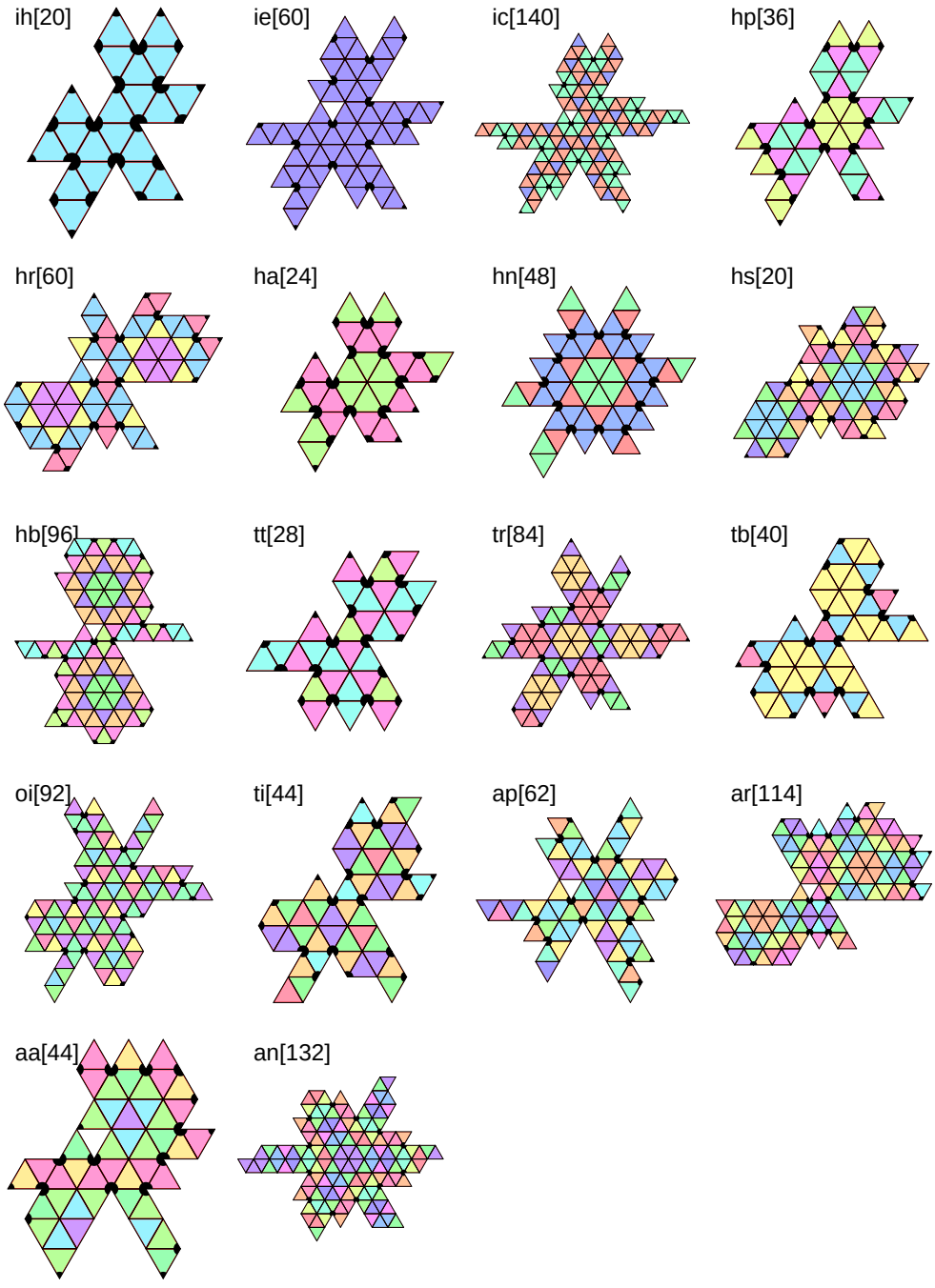

Figure 13. Developments, or 'nets' of the complete surfaces of the polyhedra that correspond to the simplest exemplars of each type of vertex-symmetric triangular-griddable polyhedron with vertex angular deficit of 60°. The labels codes are those used in the classification of Table 6.

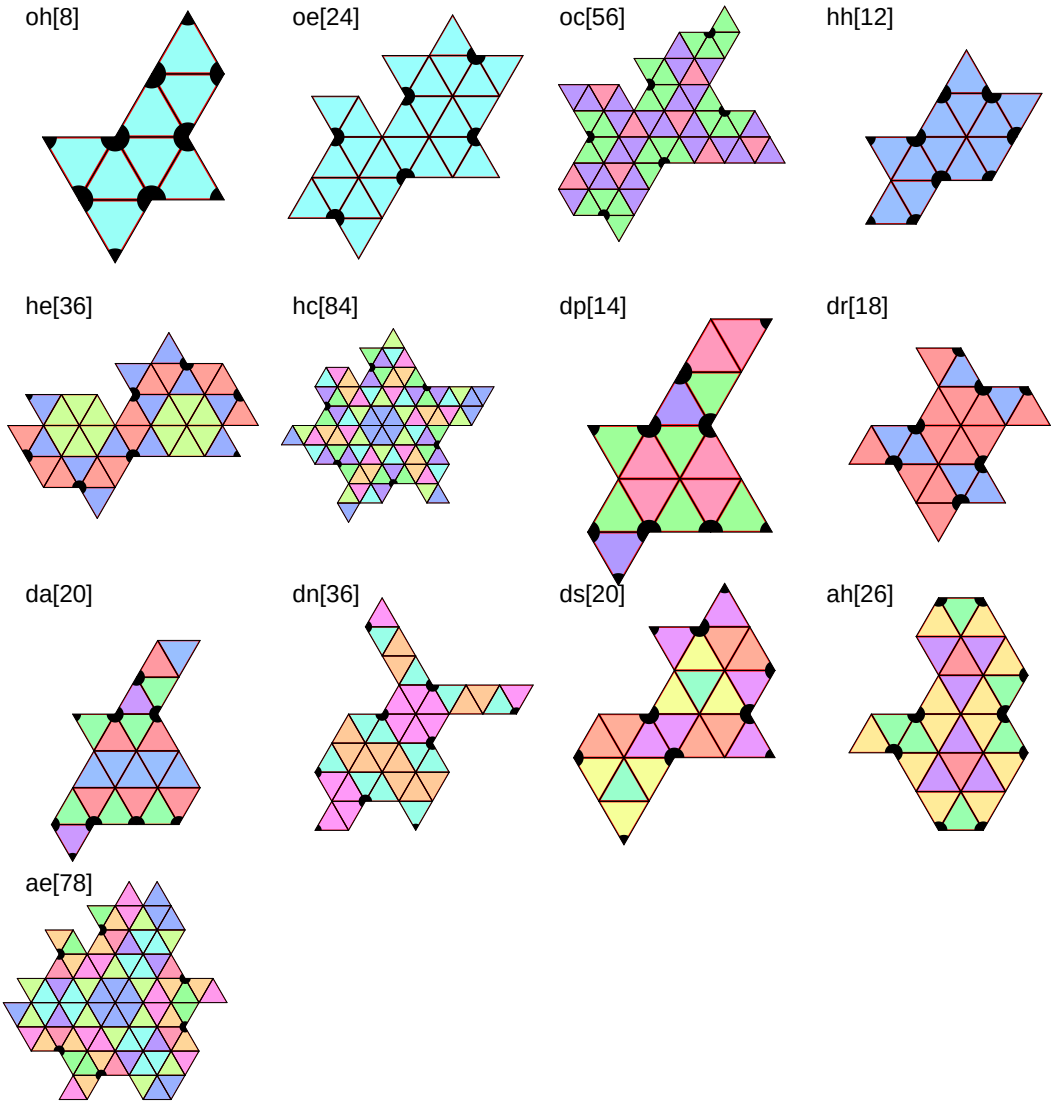

Figure 14. Like Fig. 13, but showing developments of polyhedra with vertex angular deficit of 120°.

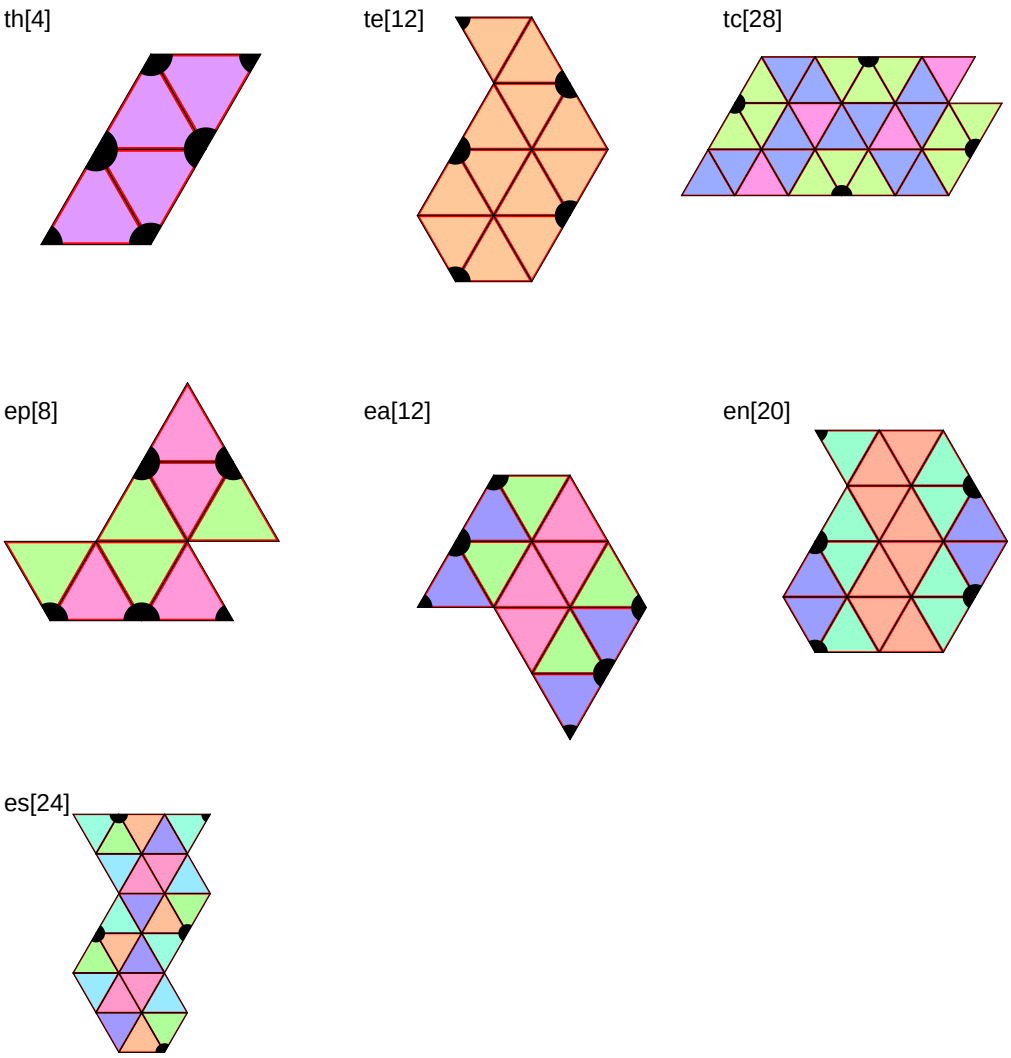

Figure 15. Like Fig. 13, but showing developments of polyhedra with vertex angular deficit of 180°.

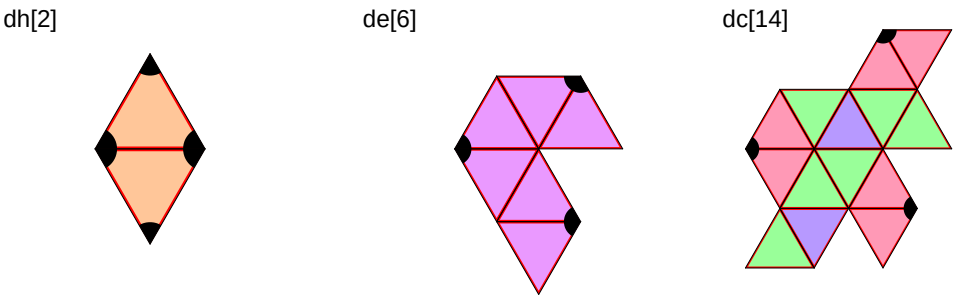

Figure 16. Like Fig. 13, but showing developments of polyhedra with vertex angular deficit of 240°.